- 1 Dynamics, predictability, impacts, and climate change considerations of the catastrophic
- 2 **Mediterranean Storm Daniel (2023)**
- Emmanouil Flaounas^{1,2}, Stavros Dafis³, Silvio Davolio^{4,5}, Davide Faranda^{6, 7, 8}, Christian Ferrarin⁹, 3
- Katharina Hartmuth¹, Assaf Hochman¹⁰, Aristeidis Koutroulis¹¹, Samira Khodayar¹², Mario Marcello Miglietta¹³, Florian Pantillon¹⁴, Platon Patlakas^{2,15}, Michael Sprenger¹, Iris Thurnherr¹ 4
- 5

- 8 1. Institute for Atmospheric and Climate Science, ETH Zurich, Zurich, Switzerland
- 9 2. Institute of Oceanography, Hellenic Centre for Marine Research, Athens, Greece
- 3. National Observatory of Athens, Institute for Environmental Research and Sustainable 10
- 11 Development, I. Metaxa & Vas. Pavlou, P. Penteli (Lofos Koufou), 15236 Athens, Greece
- 4. Dipartimento di Scienze della Terra, Università di Milano, Milan, Italy 12
- 13 5. Institute of Atmospheric Sciences and Climate, National Research Council, Bologna, Italy
- 6. Laboratoire des Sciences du Climat et de l'Environnement, UMR 8212 CEA-CNRS-UVSQ, 14
- 15 Université Paris-Saclay & IPSL, CE Saclay l'Orme des Merisiers, 91191 Gif-sur-Yvette, France
- 7. London Mathematical Laboratory, 8 Margravine Gardens, London W6 8RH, UK 16
- 17 8. LMD/IPSL, ENS, Université PSL, École Polytechnique, Institut Polytechnique de Paris, Sorbonne
- 18 Université, CNRS, Paris France
- 19 9. CNR - National Research Council of Italy, ISMAR - Institute of Marine Sciences, Venice, Italy
- 20 10. Fredy and Nadine Herrmann Institute of Earth Sciences, Hebrew University of Jerusalem,
- 21 Edmond Safra Campus, Jerusalem, Israel
- 22 11. School of Chemical and Environmental Engineering, Technical University of Crete, 73100
- 23 Chania, Greece
- 24 12. Mediterranean Centre for Environmental Studies (CEAM), Charles R. Darwin Street, 14 46980
- 25 Paterna, Valencia (Spain)
- 26 13. Institute of Atmospheric Sciences and Climate, National Research Council, Padua, Italy
- 27 14. Laboratoire d'Aérologie, Université de Toulouse, CNRS, UPS, IRD, Toulouse, France
- 28 15. Department of Physics, National and Kapodistrian University of Athens, Athens, Greece

29

31 **Abstract**

- 32 In September 2023, Storm Daniel formed in the central Mediterranean Sea as an intense
- 33 Mediterranean cyclone, causing significant socioeconomic impacts in Greece, including fatalities and
- 34 severe damage to agricultural infrastructure. Within a few days, it evolved into a tropical-like storm
- 35 (medicane) that made landfall in Libya, likely becoming, to our knowledge, the most catastrophic and
- 36 lethal weather event ever documented in the region.
- 37 This study places Storm Daniel as a centerpiece of the disasters in Greece and Libya. We aim to
- 38 conduct a comprehensive analysis that links a cyclone system with hazardous weather relevant to
- 39 extreme precipitation, floods, and significant sea wave activity. In addition, we examine Daniel's
- 40 predictability in different development stages and draw connections with previous case studies.
- 41 Finally, given the extreme precipitation produced by Daniel, we place our findings in a climatological
- 42 context to better understand its implications for numerical weather prediction and climate change
- 43 attribution.
- 44 Daniel initially developed like any other intense Mediterranean cyclone, including medicanes, due to
- 45 upper tropospheric forcing followed by Rossby wave breaking. At this stage, it produced significant
- 46 socioeconomic impacts in Greece, even in areas far from its center. As it intensified and attained
- 47 tropical-like characteristics, it peaked after landfall in Libya, where its socioeconomic impacts were
- 48 the most severe. The cyclone's formation had low predictability even at short lead times (around four
- 49 days), while the landfall in Libya was more predictable within the same lead time. Our analysis of
- 50 impacts highlights that numerical weather prediction models can capture the extreme character of
- 51 precipitation and flooding in both Greece and Libya, providing crucial information on the expected
- 52 severity of imminent flood events.

We also examine moisture sources contributing to extreme precipitation. Our findings indicate that large-scale atmospheric circulation was the primary driver, but, as Daniel matured, it drew substantial water vapor from local maritime areas within the Mediterranean. Daniel produced extreme precipitation amounts in a climatological context, fueled by a warmer Mediterranean Sea and atmosphere. Our analysis supports interpreting its impacts as characteristic of human-driven climate change but also highlights the exceptionality of this cyclone, especially in its medicane phase, which complicates the comparison with other cyclones.

1. Introduction

In September 2023, a low-pressure system developed within the central Mediterranean Sea, close to Greece. Due to the expected severity of the event, on 4 September 2023 the Hellenic National Meteorological Service named the storm 'Daniel'. Within a few days, Daniel evolved into a deep cyclone that propagated southwards, making landfall at the coast of Libya (Fig. 1a). Daniel led to substantial, unprecedented socio-economic impacts in the Central-Eastern Mediterranean from 4 to 11 September 2023, all attributed to the same weather system.

In the cyclogenesis stage, on 5 September 2023, the weather station network of the National Observatory of Athens in Greece (NOAAN; Lagouvardos et al., 2017) measured more than 750 mm of accumulated daily rainfall in the eastern part of the Thessaly region (flooded areas are shown in cyan colours in Fig. 1b) and up to 1235 mm within four days. The eastern parts of Greece experienced flooding (Fig. 1b) that led to 17 fatalities, the loss of 25% of Greece's annual agricultural production, and the destruction of the local road network. About five days later, on 10 September 2023, the cyclone made landfall near Benghazi, Libya. As a result, northeastern Libya's population of 884,000 people has been affected directly in five provinces by the collapse of two dams. About 30% of the city of Derna was flooded (Fig. 1c), and almost 900 buildings were destroyed, including road damage and other infrastructure in the area (OCHA 2023, UNICEF 2023). According to the DTM update (IOM 2023), over 5,000 people were presumed dead, 3,922 deaths were registered in hospitals, 10,000 people were declared missing by the Libyan government and Red Crescent Society, while at least 30,000 people were recognized as internally displaced (UNICEF 2023, IOM 2023) in the Derna area. Extensive damage affected critical infrastructure such as hospitals and drinking water supply systems. Many roads were rendered impassable, making it difficult for humanitarian aid and supplies. At least

Many roads were rendered impassable, making it difficult for humanitarian aid and supplies. At least \$10 million budget was allocated from the UN Central Emergency Response Fund to scale up intervention in response to the Libya disaster, and almost 72 million were requested to cope with the most urgent needs of around 250,000 people (OCHA 2023) just for the first three months after the flooding.

Daniel was an intense cyclone, preceded by Rossby wave breaking, forming an omega blocking configuration (Couto et al., 2024), and the consequent intrusion of an upper-level trough. This scenario is commonly observed before the formation of intense Mediterranean cyclones, including medicanes (Raveh-Rubin and Flaounas, 2017). From the perspective of atmospheric dynamics, upper tropospheric systems are often precursors of Mediterranean cyclogenesis. Indeed, troughs and cut-off lows correspond to stratospheric air intrusions that impose significantly high potential vorticity (PV) anomalies and thus trigger baroclinic instability (Flaounas et al., 2022). While the formation of Mediterranean cyclones is almost entirely dependent on baroclinic instability, the development and intensification of a cyclone into a deep low-pressure system is also a function of diabatic processes. More precisely, latent heat release close to the cyclone centre, mainly due to convection, is a source of positive PV anomalies at low levels, eventually translating into enhanced cyclonic circulation. Therefore, baroclinic instability and latent heat release are cyclone development's main forcings. Both processes are modulating factors of cyclones' intensification from the cyclogenesis stage until maturity, i.e., when the cyclone reaches its minimum pressure at the centre. A complete review of Mediterranean cyclone dynamics is available by Flaounas et al. (2022), while a recent thorough analysis of the dynamics of another intense cyclone in the central-eastern Mediterranean (Ianos, 2020) is provided by Pantillon et al. (2024).

As an environmental hazard, cyclones may produce heavy precipitation from the stage of genesis until their lysis, close to their centres but also in remote areas due to localized convective cells (Raveh-Rubin and Wernli, 2016), warm conveyor belts and frontal structures (Pfahl et al., 2012; Flaounas et al., 2018). Regardless of whether precipitation is stratiform or convective, the large-scale atmospheric circulation is essential for transporting water vapour toward the Mediterranean and thus "feeding" the cyclone-induced precipitation (Hochman et al., 2024). Indeed, the Mediterranean basin is composed of a relatively closed sea surrounded by high mountains. Consequently, Mediterranean cyclones have fewer water sources than their counterparts over the open oceans. In these regards, large-scale ventilation of water vapour from the Atlantic Ocean and other remote regions towards the Mediterranean has been shown in numerous cases to enhance heavy precipitation, together with local evaporation due to cyclone-induced high wind speeds (Duffourg and Ducrocq, 2011; Flaounas et al., 2019; Khodayar et al., 2021; Sioni et al., 2023). Hence, identifying and quantifying the contribution of water sources to heavy precipitation is crucial for understanding socio-economic impacts in the Mediterranean (Hochman et al., 2022a).

In a climatological context, Mediterranean cyclones produce most of the wind and precipitation extremes in the region (Nissen et al., 2010; Flaounas et al., 2015; Hochman et al., 2022b). Therefore, cyclones play a central role in the compoundness of high-impact weather events (Catto and Dowdy, 2021; Rousseau-Rizzi et al., 2023; Portal et al., 2024), also considering that landfalling systems additionally produce storm surges and significant high waves (Patlakas et al., 2021; Ferrarin et al., 2023a; Ferrarin et al., 2023b). Especially in the case of precipitation, recent results have shown that intense water vapour transport and PV streamers, as a proxy for Rossby-wave breaking, are two of the main features that lead to extreme Mediterranean events (de Vries, 2021; Hochman et al., 2023). Both of these large-scale atmospheric features favour the development of cyclones into deep, low-pressure systems (e.g., Davolio et al., 2020). Thus, their understanding is crucial for predicting socio-economic impacts on weather and climate scales.

Future trends in cyclone-induced hazards in the Mediterranean are mainly quantified through downscaling experiments (e.g., Reale et al., 2022) or statistical-deterministic methods that generate synthetic tracks (e.g., Romero and Emanuel, 2017). Nevertheless, additional investigation is needed to assess the role of climate change in the intensification of storms that occur in the current climate. While attributing extreme events, such as medicanes and high-impact extratropical storms, is a rather tricky task, recent studies based on analogues have suggested that several recent storms are more intense than expected in the absence of climate change (Faranda et al., 2022, 2023). Further investigation of this critical topic requires a case-to-case approach to take into account the particularities of each storm and to acquire a more holistic understanding of the specific processes related to cyclone intensity that are also affected by climate change.

When a high-impact weather event occurs, it encompasses multiple interconnected aspects often studied separately. First, understanding the event's dynamics and physical processes is crucial for assessing short-term forecasting and climate change implications. Second, the associated hazards—such as floods and windstorms—must be assessed concerning the specific conditions of the affected areas. This also raises questions about hazard predictability. Lastly, the event's severity must be placed within a climatological context to determine whether it produced extreme weather conditions and to attribute its intensity to climate change. Despite their interdependence, all these aspects of a specific weather event are rarely examined through an integrated approach. Our motivation is thus to apply a comprehensive framework, using Storm Daniel as the centerpiece of the September impacts in the eastern Mediterranean, and to provide an interdisciplinary assessment of the event (Shirzaei et al., 2025). In particular, we aim to address the following four questions:

- 155 1. How did cyclone development stages relate to flooding in Greece and Libya?
- How reliable and accurate were numerical models for predicting weather conditions and river discharges in relation to imminent hazards at different lead times?
- 158 3. Can numerical weather prediction models adequately simulate climate extremes?
- 159 4. Can we attribute Storm Daniel to climate change?

The following section describes the datasets and methods, while section 3 briefly describes the storm dynamics. Section 4 analyses Storm Daniel's predictability, and section 5 is devoted to Daniel's attribution to climate change.

2. Datasets and methods

2.1 Datasets

To analyze the evolution of the cyclone and assess its predictability, we use the operational analysis and the ensemble prediction system (EPS) products of the European Centre for Medium-Range Weather Forecasts (ECMWF). Since the last model upgrade at ECMWF (Cycle 48r1), operational analysis and medium-range ensemble forecast data have been available at a grid spacing of about 9 km. The increase in horizontal resolution and improvements in the data-assimilation system resulted in substantial improvements in skill (ECMWF Newsletter, 176, 2023). The EPS comprises 50 members, initialized with a perturbed analysis using slightly altered model physics and one control forecast. This probabilistic forecasting system has been designed to provide a range of possible weather conditions up to 15 days ahead, providing an estimation of predictability. Finally, to assess Daniel's climatological aspects, we used ERA5 reanalysis (Hersbach et al., 2020) with hourly atmospheric fields at a 0.25-degree grid spacing.

We used river discharge data from the Global Flood Awareness System (GloFAS; Grimaldi et al., 2022) to investigate the hydrological impacts of Daniel across Greece and Libya. GloFAS is an integral component of the Copernicus Emergency Management Service (CEMS), focusing on operational flood forecasting globally. It integrates the open-source LISFLOOD hydrological model with ERA5 meteorological reanalysis data, interpolated to align with GloFAS resolution (0.05° for version 4.0), and produced with a daily frequency. This dataset encompasses historical discharge records crucial in establishing the discharge climatology from 1993 to 2023. We employed the European Flood Awareness System (EFAS) data to assess the flood forecast potential. The EFAS system utilises the open-source LISFLOOD hydrological model, calibrated to a refined spatial resolution of approximately 1.5 km at European latitudes. Forecasts are generated twice per day, based on initializations at 00 and 12 UTC, and extend lead times from 5 to 15 days to capture a broad spectrum of potential weather conditions impacting river discharge volumes. These forecasts incorporate data from the 51 ECMWF EPS members, the Deutsches Wetter Dienst (DWD) highresolution forecasts, and the COSMO Local Ensemble Prediction System (COSMO-LEPS) with 20 ensemble members, ensuring a comprehensive analysis of the forecast potential. For this study, we used the EFAS model forecasts driven by the 51 ensemble members of the ECMWF EPS.

 Finally, to evaluate Daniel's marine and coastal impacts, we analyzed the wave results of the Mediterranean Sea Waves Analysis and Forecast (Korres et al., 2023) available via the Copernicus Marine Service (CMEMS). We also determined the wave climatology by analyzing the Mediterranean Sea wave reanalysis available via CMEMS (1993-2021; Korres et al., 2021).

2.2 Methods

2.2.1 Object diagnostics

We identify two-dimensional objects of extreme precipitation to assess the predictability of major impacts in the EPS forecasts. These objects are defined separately for each member of the EPS as neighbouring grid points where daily precipitation values exceed the 99th percentile in the ERA5 climatology (1990-2020). With these objects, we define the probability of the EPS to forecast extreme weather due to Daniel. Similarly, we define the probability of a cyclone occurrence in the EPS by identifying cyclone masks in each ensemble member as the outermost mean sea level pressure (MSLP) contour that delimits a surface smaller than that of a circular disc with a radius of 200 km.

2.2.2 Air parcel trajectories and moisture source diagnostic

231

232

233

234

235

236

237

238

239

240

241

242

243

244

245246

247

248

249

250

251

252

253

254

255

256

257

258

259

260

261

262

263

264

265

266

267

268 269

215 Ten-day air parcel backward trajectories are calculated every 20 hPa between 1000 and 300 hPa from starting locations on a regular latitude-longitude grid with a 30 km grid spacing within boxes over 216 217 Greece and Libya (as shown in Fig. 1a) using the LAGRANTO tool (Wernli and Davies, 1997; 218 Sprenger and Wernli, 2015). We calculated two sets of backward trajectories: (i) the first concerns 219 Storm Daniel, where trajectories started every 6 hours on 5 September 2023 and 11 September 2023 220 from the Greece and Libya boxes, respectively, using the six-hourly 3D wind fields from the ECMWF 221 operational analysis data; (ii) the second concerns air parcel trajectories based on the ERA5 reanalysis 222 wind fields for the 100 most extreme daily precipitation events in each of the two boxes, starting from 223 the grid points in the Greece and Libya boxes as for the first set of trajectories. These 100 extreme 224 events were the days with the highest number of grid points within the Libya or Greece region 225 experiencing daily surface precipitation exceeding the 90th percentile for autumn in 1990 - 2023. 226 Storm Daniel is among the 100 most extreme daily precipitation events for both regions. We 227 interpolated specific humidity, relative humidity, and the boundary layer height pressure along all 228 trajectories.

We identified moisture sources in Daniel and the 100 most extreme daily precipitation events using the moisture source diagnostic from Sodemann et al. (2008). This method involves the tracking of changes in specific humidity along all trajectories that precipitate upon arrival, which are defined as air parcels showing a decrease in specific humidity during the last time step before arrival and a relative humidity larger than 90% upon arrival (following Sodemann et al., 2008). Along each trajectory, an increase in specific humidity is interpreted as a moisture uptake, and a decrease in specific humidity is interpreted as a moisture loss reduces all previous moisture uptakes, weighted by their uptake amount. For a detailed description of the moisture source diagnostic, see Sodemann et al. (2008). The identified moisture uptakes along each trajectory were weighted by the decrease in specific humidity during the last step before arrival, and relative moisture uptakes over all trajectories were calculated for each six-hourly time step. Relative moisture uptakes are then gridded to a 1° global latitude/longitude grid and averaged for each day. The relative moisture uptakes are given in 10⁻⁵ % km⁻², representing each grid cell's relative contribution per km² to the precipitation in the target region. Finally, the daily relative moisture sources averaged over the 100 most extreme events are used as a climatological reference for Daniel.

2.2.3 Attribution to climate change

We used the methodology developed in the rapid attribution framework "ClimaMeter" (see Faranda et al. 2024, for more details). ClimaMeter offers a dynamic approach to contextualizing and analyzing weather extremes within a climate context. This framework provides both easily understandable, immediate contextualization of extreme weather events and more in-depth technical analysis shortly after the events. In particular, we analyze here how Mediterranean depressions landfalling in Greece and Libya have changed in the present (2001–2022; factual period) compared to what they would have looked like if they had occurred in the past (1979–2000; counterfactual period). To do so, we compute analogues of MSLP anomalies of Daniel from the MSWX database (Beck et al., 2022) and search for significant differences between present and past analogues in terms of pressure, nearsurface temperature, precipitation, and wind speed. To account for the seasonal cycle in surface pressure and temperature data, we remove the average pressure and temperature values for the corresponding calendar days at each grid point and each day. Total precipitation and wind-speed data are not preprocessed. If the duration of the event is longer than one day, we performed a moving average throughout the event on all variables. We examined all daily surface pressure data for each period. We selected the best 15 analogues, i.e., the data minimizing the Euclidean distance to the event itself, corresponding to approximately the smallest 1% Euclidean distances in each subset of our data. We tested the extraction of 10 to 20 analogues, without finding qualitatively significant differences in our results. As customary in attribution studies, the event itself is excluded for the present period. Following Faranda et al. (2022), we defined quantities supporting our interpretation of analogue-based assignments. We can then compare these quantities between the counterfactual and factual periods. The quantities are:

- Analogue Quality (Q): Q is the average Euclidean distance of a given day from its 29 closest

analogues. If the value of Q for the extreme event belongs to the same distribution as its analogues, then the event is not unprecedented, and attribution can be performed. If the Q value exceeds its analogues, the event is unprecedented and not attributable.

- Predictability Index (D): Using dynamical systems theory, we can compute the local dimension D of each SLP map (Faranda et al., 2017). The local dimension is a proxy for the number of active degrees of freedom of the field, meaning that the higher the D, the less predictable the temporal evolution of the SLP maps will be (Faranda et al., 2017). If the dimension D of the event analyzed is higher or lower than its analogues, then the extreme will be less or more predictable than the closest dynamical situations identified in the data.

- Persistence Index (Θ): Another quantity derived from dynamical systems theory is the persistence Θ of a given configuration (Faranda et al., 2017). Persistence estimates the number of days we will likely observe a situation analogous to the one under consideration.

Finally, to account for the possible influence of low-frequency modes of natural variability in explaining the differences between the two periods, we also considered the potential roles of the El Niño-Southern Oscillation (ENSO), the Atlantic Multidecadal Oscillation (AMO), and the Pacific Decadal Oscillation (PDO). We performed this analysis using monthly indices produced by NOAA/ERSSTv5. Data for ENSO and AMO were retrieved from the Royal Netherlands Meteorological Institute (KNMI) Climate Explorer. At the same time, the PDO time series was downloaded from the NOAA National Centers for Environmental Information (NCEI). The significance of the changes between the distributions of variables during the past and present periods was evaluated using a two-tailed Cramér-von Mises test at the 0.05 significance level. If the p-value is smaller than 0.05, the null hypothesis that both samples are from the same distribution is rejected, namely we interpret the distributions as being significantly different. We use this test to determine the role of natural variability.

3. Atmospheric processes leading to impacts

3.1 Cyclogenesis stage and impacts in Greece

Before Daniel formed, an omega-blocking pattern and an anticyclonic Rossby wave-breaking occurred over Europe (Couto et al., 2024). Wave breaking resulted in the intrusion of an upper-level PV streamer into the central Mediterranean basin, triggering cyclogenesis in the Ionian Sea on 4 September 2023, which eventually led to the formation of Daniel within 24 hours (northernmost, first track point in Fig. 1a). Figure 2a shows that the cyclone on 5 September 2023 was located between Italy and Greece, developing as a moderate low-pressure system with a minimum MSLP value of about 1004 hPa. The PV streamer in the upper troposphere wrapped cyclonically around the cyclone centre (green contour in Fig. 2a), pointing out an ongoing baroclinicity, forcing the cyclone's development. Accordingly, a high wind speed pattern follows the PV streamer's orientation with larger values over the Balkans and at the northwest side of the cyclone (wind barbs in Fig. 2a). This configuration summarises a typical dynamical structure of Mediterranean cyclones at a stage preceding maturity, i.e., the time of maximum intensity (Flaounas et al., 2015).

Accumulated precipitation also follows the typical structure of Mediterranean cyclones, with higher amounts on the northeast side of the cyclone centre (Flaounas et al., 2018). Figure 2a shows that at the cyclone's initial stages, the highest precipitation accumulation was observed in central Greece (Dimitriou et al., 2024). The NOAAN surface stations recorded more than 750 mm of daily rainfall and up to 1,235 mm within four days in eastern parts of the Thessaly region (flooded areas are shown in cyan colours in Fig. 1b). Notably these peak values are underestimated by about 40% in the ECMWF analysis (max IFS 24-h accumulated rainfall equal to 434 mm on 6 September 2023 00 UTC).

321 UTC)

To quantify the contribution of local and remote areas to such an intense precipitation event in Greece, Fig. 3a identifies, for the air parcels that reached the flooded area of Thessaly (blue square in

326

327

328

329

330

331

332

333

334

335

336 337

338

339

340

341

342

343

344

345

346

347

348

349

350

Fig. 3a), the areas where moisture uptake has been significant. Taking into consideration the largest moisture uptakes that contribute by at least 50% to the catastrophic precipitation in Greece (dashed black contour in Fig. 3a that primarily separates the green from the red colours), major sources were found in the Aegean and the Black Seas. This tilted southwest-to-northeast orientation of essential water sources follows the pathway of strong winds blowing over the Balkans and the eastern Mediterranean (wind barbs in Fig. 2a), having a similar orientation with the upper-level PV streamer. The intense sea surface fluxes induced by easterly winds are a precursor feature common with other cyclones developing in the same area (e.g., Miglietta et al., 2021). Further moisture mainly originated from central to eastern Europe and the North Atlantic Ocean. These source regions are in general agreement with a recent study (Argüeso et al., 2024), which investigated moisture sources of rainfall over Greece from 3 to 9 Sep 2023 using a Eulerian moisture source diagnostic. Our moisture source analysis shows larger contributions from land (54.7%) than in Argüeso et al. (2024) (27%). The Lagrangian method used in our study shows relatively large moisture contributions from north of the Black Sea because most of the air parcels arriving on 5 Sep 2023 descended and took up moisture in this region before moving southwestward along the western flank of the PV streamer. The differences in the land fraction between the two methods might originate from different periods used for the moisture source calculations, different handling of moisture uptakes above the boundary layer, a lower explained fraction of the total moisture sources (84%) with the Eulerian compared to the Lagrangian diagnostic (explained fraction of 90%), and general differences in Eulerian versus Lagrangian approaches. An ongoing comparison study of moisture source diagnostics is investigating differences in these methods in detail and will shed more light on disagreements between various moisture source diagnostics. Overall, the moisture sources agree well with the climatology of moisture sources of the Mediterranean cyclones that produce the most heavy precipitation events (Flaounas et al., 2019). The moisture sources shown in Fig. 3a largely overlap with the climatological moisture sources of extreme precipitation in the same area. However, for Daniel, they are mostly concentrated over the Aegean Sea and areas to the northeast. In contrast, the typical moisture sources for extreme precipitation in Thessaly extend further over the central Mediterranean (Fig. 3b).

351 352 353

354

355

356

357

358

359

360

361

362

363

364

365

366

367

368

The hydrological impacts of Storm Daniel were profound and unprecedented. Figure 4 compares the peak mean daily river discharge during Daniel with the historical records over three decades, integrating the cumulative hydrological impacts over the entire event. Figure 4a shows the spatial distribution of the maximum simulated peak discharge from January 1993 to August 2023 (i.e., before Daniel), demonstrating typical peak discharge patterns in the Eastern Mediterranean. On the other hand, Fig. 4b compares the event-wide mean daily peak discharge during September 2023, when Daniel occurred, against the historical peak discharges of the last 30 years in Fig. 4a. Results reveal an unprecedented magnitude of Daniel's impacts, with several areas experiencing discharges that exceeded the historical maximums by 300 to 500%. The darkest shades in Fig. 4b indicate the most heavily affected regions, where the river discharge during Daniel exceeded previous records by at least a factor of five, highlighting that Daniel was an unprecedented event of increased river discharge levels (further discussed in section 5). At this cyclone stage, 17 human casualties were registered in Thessaly, along with a profound hydrological aftermath. The extreme rainfall from 3 to 8 September 2023 led to widespread flooding across 1,150 km² in the Thessalian plain, 70% of which constituted agricultural land. The inundation severely affected the cotton crops, with floodwaters covering more than 282 km², roughly 30% of the region's total cotton fields. Over 35,000 farm animals were also affected (He et al., 2023).

369 370 371

372

373

374

375

376

377

378

379

3.2 Mature stage and impacts in Libya

Severe weather gradually faded in Greece during the night of 6 September 2023 while the surface cyclone moved southwards in phase with the upper-tropospheric low. In the following three days, Daniel lingered over the central Mediterranean Sea (circular part of the track in Fig. 1a), with minimum pressure remaining almost constant, close to 1004 hPa (Fig 1a). Figure 5a, b shows the SST anomaly in the area affected by Storm Daniel on 3 and 9 September, respectively. Before the passage of Storm Daniel, positive SST anomalies dominated the study area, with values exceeding 1°C between the Libyan coast and Greece, and lower anomalies (0 to 0.5°C) observed east of Sicily. Following the storm's passage, a significant drop in SST resulted in an extensive area of negative

anomalies greater than 1°C between Libya and Greece. A colder SST core with a decrease of less than 1.5°C was observed east of Sicily, while the northern Aegean Sea experienced an even more pronounced decline. Such SST cooling after the passage of medicanes has been previously diagnosed using explicitly resolved air-sea interactions in coupled atmosphere-ocean models (Ricchi et al., 2017; Bouin and Lebeaupin Brossier, 2020; Varlas et al., 2020) and SST observations (Avolio et al., 2024). Nevertheless, the feedback mechanism between cyclones intensity and SST cooling is expected to be less important than the one typically observed in tropical cyclones.

The role of anomalously high SSTs in intensifying cyclones has been previously shown in several studies based on numerical sensitivity experiments (Miglietta et al., 2011; Romaniello et al., 2015; Messmer et al., 2017; Pytharoulis, 2018, Argüeso et al. 2024; Sanchez et al. 2024). In the case of Daniel, deep moist convection was favoured, as suggested by the great extent of the areas covered by cold cloud-tops and intense lightning activity close to the cyclone centre (not shown). Afterward, on 8 September, the cyclone started showing tropical-like features, like deep warm core, spiral cloud bands, and a maximum wind speed in the low levels a few tens of km far from the centre. Thus, the cyclone satisfies the phenomenological definition of a medicane recently proposed (Miglietta et al., submitted). Deep convection contributed to the rapid deepening of the cyclone, which reached a minimum MSLP of 997 hPa on 10 September 2023, 18 UTC after making landfall at the northeastern coasts of Libya around 10 September 2023, 06 UTC (Fig. 1).

A comparison of Figs. 2a and 2b shows that, at the time of maturity, the area covered by at least 2 PVUs at 300 hPa is significantly smaller than during cyclogenesis. Nevertheless, Fig. 2b shows that the 2-PVU patch is collocated with the cyclone center, advected from the west. Hewson et al. (2024) proposed that this collocation is responsible for the cyclone's intensification just before landfall. In fact, the intensification of a Mediterranean cyclone due to the synergy of upper-level baroclinic forcing and deep convection is a common characteristic of intense Mediterranean cyclones, including medicanes (Flaounas et al., 2021). A previous case of a medicane intensifying due to the collocation of a PV streamer with the cyclone center was documented by Chaboureau et al. (2012). This phenomenon reflects, on the one hand, the anomalous nature of this medicane (as medicanes generally intensify over the sea and weaken inland), on the other hand, the critical role of upper-level features in the evolution of Mediterranean cyclones.

At the same time, Daniel has developed a significantly stronger MSLP gradient, leading to wind speeds that reach up to 40 knots (about 20 m s-1). The intense winds associated with the storm generated a severely disturbed sea in the Central Mediterranean basin, with south-westward propagating waves extending from the Aegean Sea to Libya following the strong winds pathway (Fig. 2b). Indeed, the analysis of the wave data from the Mediterranean Sea Waves Analysis and Forecast evinces waves with significant height of about 5 m in the Gulf of Sirte and the northern Aegean Sea (Fig. 6a). Such values exceed the 99th percentile in the Mediterranean Sea wave reanalysis. A peculiar aspect of Daniel is that strong winds blew in the Central Mediterranean Sea for many days. As a result, Daniel preserved a severe sea state over northern Greece, in the Central Mediterranean basin, and along the Libyan coast. To evaluate the cumulative impact of the event, we computed the total storm wave energy (TSWE; Arena et al., 2015) by integrating the wave power contribution of each sea state over the storm duration (Fig. 6b). TSWE reaches peak values of about 3000 kWh m⁻¹ in the Gulf of Sirte, which is above the 99th percentile of the total storm wave energy obtained from the Mediterranean Sea wave reanalysis. Such an energetic sea condition and the storm surge affected much of Libya's eastern coastal zones, causing coastal flooding, erosion, and infrastructure damage (World Bank, 2023).

In terms of precipitation, Storm Daniel also presented exceptional features. During the cyclone's mature stage, Bayda experienced about 414.1 mm of rainfall within less than 24 hours, equaling 80% of the city's mean annual accumulated precipitation and a new daily precipitation record (Weather World Meteorological Organisation, 2023). It is worth mentioning that simulated 24-hr total accumulated precipitation on 11 September 2025 in Libya, up to 382 mm, was not located within the Derna catchment, as it has been discussed in Hewson et al. (2024), which was the most impacted area.

Significant moisture sources (red colours in Fig. 3c) encompass the cyclone centre with more than 50% of the moisture originating from the Mediterranean Sea. This suggests that the cyclone-induced circulation played an essential role in moistening the atmosphere within the proximity of the cyclone. Nevertheless, the largest moisture sources that contribute together to at least 50% of the total precipitation in Libya (black dashed contour encompassing green to red colours in Fig. 3c) still retain a southwest-to-northeast orientation as in Fig. 3a (i.e., during the precipitation event in Greece). Comparing the moisture sources among the two precipitation events in Greece and Libya, the cyclone tends to attract more moisture from its surrounding area in the latter case. In contrast, in both cases, northern moisture sources tend to align with the large-scale circulation responsible for downstream cyclogenesis in the Mediterranean. This southwest-northeast orientation of moisture sources contrasts with the climatological sources in Figs. 3b and 3d, mainly highlighting the importance of local sources, especially from the Mediterranean Sea westwards of the two study regions.

Figure 4 highlights the exceptional river discharges in the region, as in the case of Greece. However, the absence of similarly strong discharge signals in several severely impacted regions, such as the wider Pelion area in Greece and Derna (Libya), is notable and can be attributed to several factors. First, the GloFAS model has limitations in spatial resolution and calibration. The model operates at a resolution of approximately 5 km (0.05°), which, while adequate for global-scale flood awareness, is insufficient for resolving localized hydrological dynamics. For instance, the catchments east of Volos, including the wider Pelion area, are approximately 30 km2, while the Derna basin spans around 575 km2. In both cases, localized rainfall-runoff dynamics are critical in shaping discharge patterns, particularly during extreme events. Due to insufficient in-situ discharge data, the absence of Greece and Libya in the GloFAS calibration dataset further exacerbates these limitations since the model relies on generalized parameter regionalization rather than site-specific calibration, introducing significant uncertainties into discharge predictions. Furthermore, inaccuracies in the rainfall inputs depicted in Figure 2 propagate into the discharge simulations shown in Figure 4. For instance, within the Peneus catchment, the maximum recorded 24-hour accumulated precipitation was 274 mm at Zappeio and 226 mm at Neraida stations, as Dimitriou et al. (2024) reported, while accumulations of up to 750 mm were recorded outside the catchment, specifically over the Pelion area, east of Volos. In the Wadi Derna catchment, extreme rainfall exceeded 400 mm day-1, with torrential rainfall ranging between 150 and 240 mm across several locations and Al-Bayda recording a maximum of 414.1 mm (WMO, 2023). These rainfall extremes were underrepresented in the GloFAS rainfall inputs, propagating into the discharge simulations and contributing to the muted signals observed in Figure 4(b).

4. Weather forecasting of Daniel and implications for impacts

Daniel's impacts took place in two distinct periods: during cyclogenesis and at maturity. In the former stage, most precipitation was produced in areas far from the cyclone centre, drawing moisture from the surrounding areas. At the later stage, the cyclone impacts were relevant around landfall, and precipitation and sea level rise were important close to the cyclone centre. Therefore, the two distinct stages of Daniel that provoked substantial impacts in Greece and Libya were linked to cyclone stages of different dynamics, which also have other implications in Daniel's numerical prediction. In the case of Greece, i.e., at the initial stage of Daniel, it is the timely prediction of cyclogenesis that would have primarily provided useful information to civil protection, whereas, in the case of Libya, it would have been the accurate prediction of the cyclone track, intensification, and its landfall location. This section focuses on the predictability of the environmental hazards linked to Daniel's socio-economic impacts, i.e., precipitation amounts, sea state, and cyclone track.

4.1 Forecasting cyclogenesis stage

Concerning the cyclogenesis stage, a forecast model has to predict the formation of the cyclone to provide valuable information regarding its impact. This suggests that numerical weather prediction models should accurately reproduce the large-scale atmospheric circulation, the Rossby wave breaking, and the consequent intrusion of the PV streamer within the Mediterranean, as shown in Fig. 2a by the green contour. Such a large-scale circulation pattern is absent from forecasts initialised one week ahead (Fig. 7a). At a lead time of 120 hours, the PV streamer is present but with high

uncertainty among the EPS members on its location (Fig. 7c). Indeed, the PV distribution of all EPS members at 300 hPa (outlined by coloured crosses in Fig. 7) depicts a much larger area of possible high PV values than the one in Fig. 2a. This is due to the limited agreement on the occurrence -or colocation- of the intrusion of the PV streamer among the EPS members, of the order of 25 to 50%, as suggested by the blue crosses in Fig. 7c.

Following the uncertainty in the PV streamer occurrence, the cyclone is also absent from the MSLP ensemble average one week ahead (black contour in Fig. 7a) and the MSLP spread seems rather consistent within the shown domain (about 1 to 3hPa). At subsequent lead times, higher spread of MSLP tends to concentrate close to the cyclone centre (Figs 7c and 7e) until it becomes negligible 24 hours before cyclogenesis (Fig. 7g). At such a short lead time, the cyclone formation was forecast with confidence to occur in the Ionian Sea, to the southwest of Greece (black contours in Fig. 7g). Confident forecasts of cyclogenesis should go hand in hand with higher agreement among the EPS members on the location of the PV streamer. Indeed, 24 hours before cyclogenesis, more than 95% of EPS members agreed on the area of PV streamer intrusion. Accordingly, average values (blue contour in Fig. 7g) better match the ones in the ECMWF analysis (green contour in Fig. 2a).

To get deeper insights into the representation of cyclogenesis among the EPS members, Fig. 8 shows the level of agreement on the cyclone objects (as presented in section 2.2.1). At a lead time of 168 hours, cyclogenesis forecast was rather poor (Fig. 8a), but at a lead time of 120 hours (Fig. 8c), cyclone centres are present (red dots in Fig. 8), scattered in the central Mediterranean but still close to the actual location where the cyclone initially formed. Higher overlapping of cyclone objects among the EPS members (green shading in Fig. 8) is indeed within the limits of the observed cyclone object as in the ECMWF analysis (black contour in Fig. 8c). In fact, about 30% of the different EPS members produce overlapping cyclone objects. At a forecast lead time of three days, the overlapping of cyclone objects increases clearly (comparing green shaded areas between Figs 8c and 8e), suggesting higher agreement among the EPS members on the cyclone occurrence within the correct location. The high agreement is retained also for shorter lead times (Fig. 8g).

The similar behaviour in the cyclone and PV streamer predictability relies on the direct relationship between the Rossby wave breaking over the Atlantic Ocean and the accurate prediction of Mediterranean cyclogenesis. This has been highlighted by Chaboureau et al. (2012) and Pantillon et al. (2013) for the case of the extratropical transition of a hurricane upstream of a medicane, more recently by Portmann et al. (2020) for another case and has been demonstrated by Sherrmann et al. (2023) in a semi-idealized framework. In the case of Daniel, Hewson et al. (2024) similarly suggested the role of the extratropical transition of Hurricane Franklin as responsible for the high uncertainty one week ahead. Only in forecasts initialized after the extratropical transition has occurred is the PV streamer predicted to intrude on the Mediterranean, thus explaining the contrast between 5 and 7 days lead times. A similar "jump" in the predictability of cyclone occurrence has been shown for several medicane cases by Di Muzio et al. (2019). Most probably, this "jump" is due to the dependence of Mediterranean cyclogenesis on the preceding Rossby wave breaking and, consequently, on the credible inclusion of this event within the forecast initial conditions.

4.2 Forecasting cyclone location and intensity at the mature stage

Figure 1a shows that on 10 September, Daniel made landfall on the coasts of Libya. For all different forecast lead times of this event, the spread of MSLP consistently retains high values close to the landfalling area (right column of panels in Fig. 7). This is directly relevant to the high MSLP gradients close to the cyclone centre (Fig. 2b) where negligible displacement of cyclone centres may result in a relatively large standard deviation of MSLP in the EPS. Indeed, Figs. 8b and 8d point to the high certainty of the cyclone occurrence in the EPS, where most members produce consistent and overlapping cyclone objects (depicted by dark green shading). Such performance comes in contrast to forecasting the stage of cyclogenesis, where MSLP spread does not have a clear pattern (the left panels of Fig. 7, green and yellow areas), and cyclone objects present limited overlapping for the same lead times (e.g., comparing Figs 8c and 8d). The limited agreement among the EPS members on the PV streamer intrusion leads to considerable differences among the EPS members on the location

or even the occurrence of cyclogenesis. In contrast, the predictability of landfall in Libya seems more consistent among the EPS members of ECMWF.

Considering a forecast lead time of 120 hours (i.e., initialization on 6 September), the cyclone has already formed and was located over the central Mediterranean (just before the spiral part of the track). Therefore, the cyclone has already been inscribed in the model's initial conditions. Still, from the perspective of impacts, the location of landfall and the cyclone's intensity are crucial. Figure 9a shows that even for an early lead time of five days (initial conditions of 5 September 2023, 0000 UTC), the cyclone tracks from all EPS members make landfall on the Libyan coasts. The spread of the tracks is wide enough to include the actual cyclone track (in blue colour in Fig. 9a); therefore, the forecast may lead to a reliable and timely warning of potential impacts.

Nevertheless, Fig. 9b shows that almost all the EPS members underestimated the cyclone's intensity by forecasting too high MSLP values on 10 September at the time of landfall. The intensity of the cyclone is dependent on the baroclinic and diabatic forcing of its development (Flaounas et al., 2021). Therefore, the performance of all EPS members depends on the accurate representation of the parametrized processes, mainly convection close to the cyclone centre and surface fluxes, and the morphology of the PV streamer intrusion. For the present case, Hewson et al. (2024) noted that, while in the development stage the latent heat released from convection, favoured by the high SST and intense sea surface fluxes, balanced out the tendency for frictional decay, in the last stage a marked upper-level low moving from the west (marked by high PV values in Fig. 7h) was responsible for a further deepening. Upper tropospheric forcing is crucial in accurately predicting cyclone intensity in this context. While Fig. 7b —unlike Fig. 7a— shows that some EPS members align with the location of this upper tropospheric feature (blue crosses), an average of 2 PVU and an agreement above 50% among the EPS members near the cyclone center is only evident at a lead time of approximately three days (Fig. 7f, depicted by green crosses).

5. Daniel's impacts in a climatological context

5.1 Forecasting climate extremes

The previous sections focused on the capacity of the EPS to forecast Daniel cyclogenesis as the primary driver of impacts. In this section, we extend this analysis by focusing on the predictability of hazards in a climatological context, namely extreme precipitation and consequent floods. We used the ERA5 reanalysis to diagnose extremes since this product offers a reliable and consistent representation of present-day climate (Hersbach et al., 2020). In this respect, the left column of Fig. 10 shows the area affected by extreme daily precipitation on 5 September (in red contour, explained in Section 2.2.1). In addition, Fig. 10 shows the percentage of the EPS members that forecast daily precipitation exceeding the climatological threshold for extremes, defined by the 99th percentile of daily precipitation in ERA5 (in blue shading). At a lead time of 120 hours (Fig. 10c), less than half of the ensemble members predicted the climatological extreme precipitation amounts within the area delimited by the climatological values of ERA5 (red contours). Nevertheless, the area formed by the blue shading in Fig. 10c is consistent with the climatological extremes. It seems that the members of the EPS that produce extreme precipitation could provide information on the potential occurrence of high-impact weather at least five days in advance. Therefore, accurately forecasting the time and location of cyclone formation (as shown in Fig. 8) may play a secondary role in predicting its impacts in Greece. In this context, the reliable simulation of moisture inflow—which appears to be more closely linked to large-scale circulation, as previously discussed—by the EPS members could be more crucial for impact prediction.

Interestingly, the overlap of extreme precipitation objects among the EPS members might exceed 70% in the area of Thessaly in Greece for a lead time of even 120 hours (Fig. 10c). This percentage is significantly higher than the maximum percentage of overlap between the cyclone objects (Fig. 8c). This suggests that the EPS members have been more consistent in the production of extreme precipitation even if cyclone centres presented a comparably greater spread. For subsequent lead times, the predictability of extreme precipitation strongly increases, showing a high probability for a

lead time of 72 hours. Indeed, almost all members predict extreme precipitation off the coast and in the northeastern part of Greece within the eventually flooded area of Thessaly.

When Daniel made landfall and produced impacts on the Libyan coasts, the EPS showed higher predictability, with cyclone objects and associated extreme precipitation being predicted at least five days in advance by several EPS members (Fig. 10d), albeit the location of both cyclone and precipitation objects are still displaced to the southwest compared to the analysis (Figs. 8d and 10d). This comes in accordance with the southern displacement of several ensemble member tracks in Fig. 9a. The probability strongly increases at shorter lead times (Figs 10f and 10h) mostly and all EPS members tend to converge to similar cyclone locations when reaching a lead time of one day (Fig. 8h).

The potential of extreme precipitation leading to substantial socio-economic impacts has also been transferred to hydrologic discharge forecasts. The hydrographs presented in Fig. 11 examine river discharge predictability as forecast by the operational European Flood Awareness System (EFAS) during Daniel. For the Peneus River outlet in Thessaly, the forecast initiated on 1 September underpredicted the peak discharge on 5 September. Nevertheless, extreme discharges were evident for several members five days in advance. The forecast accuracy improved getting closer to the event, with ensemble members (grey stripes) converging towards the peak discharge ("perfect forecast" - red line). This trend indicates an increasing reliability of the forecast as the lead time decreases, particularly within 48 hours of the event. The skill in discharge predictability for the Peneus River can be attributed, in part, to the large size of the basin (11.063 km²), which aligns relatively well with the spatial resolution of the EFAS model, enabling an accurate representation of distributed hydrological processes and moderating runoff variability.

The forecasts for the Wadi Derna River outlet (Fig. 11, right panels) exhibit significant variability and fail to converge during the earlier forecast initialization dates as well as at shorter lead times. This persistent lack of convergence can be attributed to distinct challenges of both temporal scales. For earlier forecast initialization dates, the primary source of variability lies in the westward displacement of extreme precipitation predicted by the EPS (Figs. 10b and 10d). For example, forecasts initialized on 9 September, during a critical period for implementing preventative measures, display a wide spread and a shortfall in the median forecast compared to the benchmark (red line). This variability persists even for forecasts initialized on 10 September. The failure to converge at shorter lead times is compounded by challenges inherent to the Wadi Derna catchment. The resolution of the precipitation forcings used in the forecasts combined with the relatively small size (575 km2) and flash-flood-prone nature of this basin amplify the uncertainties in predicting discharge, particularly in response to localized extreme rainfall.

Figure 4 provides critical context by comparing the peak mean daily river discharge during Storm Daniel with the historical baseline. The unprecedented magnitude of the event is evident in Fig. 4b, where discharges exceeded the historical reanalysis by at least fivefold in certain regions. However, the relatively weak signal for the Wadi Derna catchment underscores the limitations of the GloFAS and EFAS systems in accurately resolving runoff dynamics in smaller basins. This discrepancy is primarily attributed to insufficient model resolution, inaccuracies in rainfall inputs, and the lack of detailed hydrological calibration for these catchments. In contrast, the much stronger signal observed in the Peneus catchment aligns with larger basin sizes and better-resolved hydrological processes, where models more effectively captured the extreme nature of the event.

The ability of EFAS to predict extreme events, as shown in Fig. 11, highlights its value in forecasting severe hydrological impacts. However, discrepancies in simulated peak discharge remain apparent, such as the overestimation of runoff for the Peneus River outlet. EFAS simulated peak discharge at approximately $5000 \text{ m}^3 \text{ s}^{-1}$, whereas observed values, based on station-level data and H-Q curve estimates, were less than $2000 \text{ m}^3 \text{ s}^{-1}$ (Dimitriou et al, 2024). This overestimation reflects inherent limitations in the model's spatial resolution and hydrological representation. Furthermore, the absence of flood protection infrastructure, such as levees or dams that attenuate runoff and peak flows is not

accounted for in the EFAS and GloFAS systems, contributing to these discrepancies. Additionally, the simplified representation of retention processes, including floodplain storage and wetland buffering, further amplifies discharge estimates in some regions. For smaller basins such as Wadi Derna, the rapid hydrological response to localized extreme rainfall presents additional challenges. The variability in rainfall distribution, coupled with the model's limited ability to capture localized hydrological dynamics, results in a weaker signal for the catchment, even during an event as extreme as Storm Daniel. These limitations emphasize the need for improved model resolution, enhanced precipitation forcings, and better calibration tailored to local catchment characteristics.

Nonetheless, the ability of EFAS to predict extreme discharges, particularly within short lead times, demonstrates the potential of operational forecast systems in capturing the extreme values of such events. Supported by EFAS and GloFAS, the Copernicus Emergency Management Service (CEMS) provides critical insights into the timing and magnitude of extreme hydrological events. These forecasts are vital for enhancing preparedness and response strategies in the face of escalating climate extremes, offering essential tools for civil protection efforts and mitigating the socio-economic impacts of such disasters.

5.2 Attribution to climate change

We assess Daniel's attribution to climate change using ClimaMeter's analogue-based approach (Faranda et al., 2024). By comparing surface pressure patterns in the periods 1979–2000 ("past") and 2001–present ("current"), we identify how similar Mediterranean depressions have evolved. We use MSWX data to analyze changes in temperature, precipitation, and wind speed associated with these analogues, attributing observed shifts to anthropogenic climate change. We repeat the analysis twice, once for 5-6 September, when Daniel impacted Greece, and once for 10-11 September, when Daniel impacted Libya.

About impacts in Greece, we search analogues for 5 September 2023 within the region defined within the domain shown in Fig. 12a and within the extended autumn season from September to December (SOND). Figure 12a-d shows that cyclone systems similar to Daniel impacting Greece have about the same order of pressure minima in their centre as they did in the past. Figure 12e-h shows that temperature during depressions has increased in the Ionian Sea by about 2°C and decreased over Anatolia. Precipitation analysis (Fig. 12j-l) shows that similar events produce heavier precipitation over the Ionian Sea and Albania but generally lower precipitation amounts over continental Greece and the Peloponnese (between 4 and 12 mm day-1). The metrics Q, D, and Θ (Figs 12q-s) are computed to discuss changes in the possible dynamical properties of the eventTo. Figs 12q-s show no significant changes between the two periods (present and past climate). We can, however, infer how close the event is to its analogues using the metric Q, which further highlights that the event has similar analogues in past and present periods. We also find that similar events have become more frequent in December, while they previously occurred mainly in October (Fig. 12t). To evaluate the possible role of low-frequency modes of natural variability in explaining the differences between the composite maps of analogues in the two periods, we compare the distributions of the ENSO, AMO, and PDO values on the dates of the analogues in the past and present periods, and we test the statistical significance of the observed differences. For this date, our analysis suggests that natural climate variability, particularly the AMO and PDO, may have influenced the development of the MSLP pattern associated with the storm (Figs. 12u-w). To clarify the trend in the frequency of these events, Fig. 12x considers in each period 30 analogues instead of 15, showing an increase in their number.

We repeat the analysis for 10-11 September 2023 within the region depicted in Fig. 13a and search for analogues for SOND. Results are reported in Fig. 13. The MSLP changes (Fig. 13d) show no substantial differences in the areas significantly affected. The temperature changes (Fig. 13h) reach $+2^{\circ}$ C warmer temperatures on the east part of the domain. Precipitation changes (Fig. 13l) indicate that similar events produced higher precipitation amounts along the eastern Libyan coast (between 5 and 9 mm day-1), which experienced intense rainfall from Daniel on 10 September 2023. The metrics Q, D, and Θ (Figs. 13q-s) show no significant differences between the two periods. While the 5

September analysis of Q identified suitable analogues, here, Q indicates that no good analogues are available, underscoring the exceptional nature of Daniel's pressure pattern when the storm impacted Libya. Events have become less frequent in September and November and slightly more common in December (Fig. 13t). As for 5 September, we find that AMO and PDO may have influenced the development of the MSLP pattern associated with the storm (Figs. 13U-w). Figure 13x showed changes in the frequency of these events when 30 analogues were searched for the entire period analyzed. As in the case of impacts in Greece, a significant increasing trend in frequency is found.

The analogues method helps us understanding extreme weather events like Daniel by comparing them to similar past events and seeing how they have changed over time. This allows us to assess whether climate change has influenced the storm's characteristics. While large-scale climate variability modes such as ENSO, AMO, and PDO can influence atmospheric conditions, our analysis does not establish a direct causal link between these modes and the development of Daniel; instead, this assessment is exploratory, highlighting potential associations without making definitive attributions given the limitations of a 40-year dataset.

For 5 September, when Daniel impacted Greece, we found similar past Mediterranean storms, suggesting that this part of the storm's track was unusual but not unprecedented. Since we see no major changes in the MSLP pattern, the increase in precipitation over the region is most likely linked to higher sea surface temperatures (SSTs), which provide more moisture to the atmosphere. This matches other studies that show Greece experienced particularly strong moisture anomalies.

For 10-11 September, when Daniel reached Libya, our method found no suitable past matches, highlighting the exceptional nature of the storm's pressure pattern at this stage. However, like in Greece, we do not see substantial changes in MSLP, meaning that the increase in rainfall over Libya was also likely driven by warmer SSTs and a warmer atmosphere, which can hold more water (Clausius-Clapeyron relationship) rather than a shift in atmospheric dynamics patterns. The MSWX dataset provides a reliable representation of large-scale atmospheric patterns but does not fully capture localized extreme precipitation intensities, which explains why our figures underestimate the observed rainfall totals, particularly in Libya; therefore, our analysis should be interpreted as reflecting broader climatological trends rather than exact station-level extremes. Importantly, while Daniel brought heavy rainfall, the disaster in Derna was mainly caused by the failure of poorly maintained dams (Shirzaei et al., 2025). Dente et al. (2024) confirm this, showing that while rainfall was intense, it was not so extreme to explain the scale of destruction—factors like unsafe building locations and poor emergency response played a major role. These considerations underscore a key point: while climate change can amplify precipitation by increasing SSTs, the most severe impacts often depend on societal factors such as infrastructure resilience and disaster preparedness.

6. Summary and conclusions

In the last decade, more than 410,000 deaths have been attributed to weather-related disasters, mostly in low-income countries where heatwaves and intense precipitation events are the leading causes of death. Aside from human casualties, 1.7 billion people have been affected in the 2010-2020 decade by these kinds of phenomena. The IFRC World Disasters Report (2020) concluded that the climate acts as a risk multiplier, especially in the case of low-income countries and at a regional level therein. A glaring example of the impact of such disasters has been highlighted by the recent floods in the Mediterranean, especially in Greece and Libya, following the Mediterranean cyclone Daniel.

This study aimed to comprehensively analyze medicane Daniel, which links atmospheric dynamics, predictability, and impacts. Beyond the description of the underlying physical processes, atmospheric dynamics are used here to understand the performance of numerical weather prediction models. Impacts, in terms of floods and sea state (for Libya), have also been analyzed concerning numerical weather prediction models. Our analysis has been framed by the climatological context of cyclone-induced precipitation and relevant impacts that link with climate change attribution of both catastrophic events.

 From the perspective of atmospheric dynamics, the processes governing Daniel were similar to those identified for other intense Mediterranean cyclones: cyclogenesis was triggered by the intrusion of an upper-level PV streamer in the Ionian Sea, and thereafter, the cyclone developed into a deep storm, that propagated southwards and towards Libya while it was turning into a well defined mesoscale tropical-like cyclonic system. Regarding impacts, we identified two well-distinct stages: the first is relevant to cyclogenesis, where Daniel was newly formed and affected Greece with severe floods (on 5 September 2023). In the second stage, Daniel reached maturity while making landfall in Libya, where it inflicted severe socio-economic impacts on 10 September 2023 due to floods (about 5 days after the floods in Greece). Daniel produced extreme precipitation in both stages, driving a moisture flow towards the areas that experienced the floods. The moisture transport followed the large-scale atmospheric circulation with large amounts of moisture that contributed to the catastrophic precipitation in the flooded areas were drawn locally from the Mediterranean Sea, which has been anomalously warm, but also from the continental regions of central and eastern Europe.

In Greece, the floods occurred relatively remotely from the cyclone centre. On the other hand, floods in Libya occurred close to the cyclone centre. Therefore, the implication of different cyclone dynamics is important in predicting socio-economic impacts at both weather and climate scales. During its first stage in Greece, the predictability of the cyclone formation was relatively poor for lead times of more than four days. It was a rather challenging issue for the ECMWF EPS to forecast precisely the intrusion of the PV streamer in the Mediterranean. This result aligns with previous studies that showed relatively poor performance in predicting medicane occurrences for lead times of the order of four to five days (Di Muzio et al., 2019). With higher confidence, the ECMWF EPS could forecast cyclogenesis, and thus the flooding event, for shorter lead times.

During its second stage (impacts in Libya), the cyclone intensified quickly, transitioned into a medicane, and made landfall in Libya within a few days. The predictability of the medicane track -and therefore its landfall- showed higher certainty for lead times of four days. This suggests that numerical weather prediction models are more prone to an erroneous predictability of the stage of cyclogenesis, i.e., after the cyclone formed, it is more likely for a forecast model to correctly predict correctly its evolution in terms of location.

Precipitation amounts were found to correspond to climate extremes in both countries, Greece and Libya, where floods were responsible for unprecedented river discharges that largely exceeded the climatological maxima of the last 20 years. The numerical weather prediction model could forecast these climate extremes (even if thresholds were defined by reanalysis and not by the same forecast model). This suggests the exceptional potential for information to the public about the severity of imminent high-impact weather. Indeed, framing weather forecasts into a climatological context, e.g., providing a precipitation event return period, would provide the means to the local population for an empirical assessment of the severity of an imminent high-impact weather event. In this context, we have analyzed Daniel concerning climate change and provided the grounds to interpret Daniel as an event whose characteristics can be ascribed to human-driven climate change. In these regards, we have performed an analysis based on analogues; indeed, several cyclones with similar characteristics were found during winter. The anomalous occurrence of such a storm in September, a warmer month for SST, could be a reason for enhancing its destructiveness through enhanced precipitation.

In the scientific literature, weather events are typically analysed as case studies with specific objectives that rarely escape the narrow scope of a single scientific discipline. Here, we used Daniel, a high-impact weather event, as a centrepiece of different approaches to better understand socioeconomic impacts through the prism of both weather and climate scales. We find such an approach valuable for bridging different scientific communities and eventually important for communicating hazards to the local population. We envisage using this interdisciplinary approach for other weather extremes and regions.

Acknowledgements

819 We gratefully acknowledge Ambrogio Volontè and an anonymous reviewer for accurately reviewing 820 our paper. This article is based upon collaborative work of two COST Actions: CA19109 821 "MedCyclones" and CA22162 "FutureMed", supported by COST – European Cooperation in Science 822 and Technology (http://www.cost.eu, last access: 14 February 2025) and from project "Earth 823 Observations as a cornerstone to the understanding and prediction of tropical like cyclone risk in the Mediterranean (MEDICANES)", ESA Contract No. 4000144111/23/I-KE. Georgios Kyros from the 824 825 National Observatory of Athens/meteo.gr is acknowledged for helping collect the Copernicus 826 Sentinel-2 data in Figure 1. The Israel Science Foundation (grant \#978/23) funds AH's contribution. 827 PP was funded by the EU's Horizon Europe program, OCEANIDS (G.A. No. 101112919). SD 828 acknowledges the support from Next Generation EU, Mission 4, Component 1, CUP 829 B53D23007490006, project "Exploring Atmospheric Rivers in the Mediterranean and their 830 connection with extreme hydrometeorological events over Italy: observation, modelling and impacts 831 (ARMEX)". We thank Franziska Aemisegger for providing the msd-cpp code for the calculation of 832 the moisture sources.

833 834

7. References

Argüeso, D., Marcos, M. and Amores, A.: Storm Daniel fueled by anomalously high sea surface temperatures in the Mediterranean, npj Clim Atmos Sci 7, 307, https://doi.org/10.1038/s41612-024-00872-2, 2024.

837 838 839

840

835

836

Avolio, E., Fanelli, C., Pisano, A. and Miglietta, M. M.: Unveiling the relationship between Mediterranean tropical-like cyclones and rising Sea Surface Temperature. Geophysical Research Letters 51, e2024GL109921, https://doi.org/10.1029/2024GL109921, 2024.

841 842 843

844

845

Beck, H. E., Van Dijk, A. I. J. M., Larraondo, P. R., McVicar, T. R., Pan, M., Dutra, E., and Miralles, D. G.: MSWX: Global 3-Hourly 0.1° Bias-Corrected Meteorological Data Including Near-Real-Time Updates and Forecast Ensembles, Bulletin of the American Meteorological Society, 103, E710–E732, https://doi.org/10.1175/BAMS-D-21-0145.1, 2022.

846 847 848

Bouin, M.-N. and Lebeaupin Brossier, C.: Impact of a medicane on the oceanic surface layer from a coupled, kilometre-scale simulation, Ocean Sci., 16, 1125–1142, https://doi.org/10.5194/os-16-1125-2020, 2020.

850 851

849

Catto, J. L. and Dowdy, A.: Understanding compound hazards from a weather system perspective, Weather and Climate Extremes, 32, 100313, https://doi.org/10.1016/j.wace.2021.100313, 2021.

854

Chaboureau, J., Pantillon, F., Lambert, D., Richard, E., and Claud, C.: Tropical transition of a Mediterranean storm by jet crossing, Quart J Royal Meteoro Soc, 138, 596–611, https://doi.org/10.1002/qj.960, 2012.

858

Couto, F. T., Kartsios, S., Lacroix, M., and Andrade, H. N.: A Quick Look at the Atmospheric Circulation Leading to Extreme Weather Phenomena on a Continental Scale, Atmosphere, 15, 1205, https://doi.org/10.3390/atmos15101205, 2024.

862

Davolio, S., Della Fera, S., Laviola, S., Miglietta, M. M., and Levizzani, V.: Heavy Precipitation over Italy from the Mediterranean Storm "Vaia" in October 2018: Assessing the Role of an Atmospheric River, Monthly Weather Review, 148, 3571–3588, https://doi.org/10.1175/MWR-D-20-0021.1, 2020.

866

De Vries, A. J.: A global climatological perspective on the importance of Rossby wave breaking and intense moisture transport for extreme precipitation events, Weather Clim. Dynam., 2, 129–161, https://doi.org/10.5194/wcd-2-129-2021, 2021.

870

Dente, E., Armon, M., and Shmilovitz, Y.: The September 2023 flood in Derna, Libya: an extreme weather event or man-made disaster?, EGU General Assembly 2024, Vienna, Austria, 14–19 Apr

32

- Di Muzio, E., Riemer, M., Fink, A. H., and Maier-Gerber, M.: Assessing the predictability of Medicanes in ECMWF ensemble forecasts using an object-based approach, Quart J Royal Meteoro
- 877 Soc, 145, 1202–1217, https://doi.org/10.1002/qj.3489, 2019.

Dimitriou, E., Efstratiadis, A., Zotou, I., Papadopoulos, A., Iliopoulou, T., Sakki, G.-K., Mazi, K., Rozos, E., Koukouvinos, A., Koussis, A. D., Mamassis, N., and Koutsoyiannis, D.: Post-Analysis of Daniel Extreme Flood Event in Thessaly, Central Greece: Practical Lessons and the Value of State-of-the-Art Water-Monitoring Networks, Water, 16, 980, https://doi.org/10.3390/w16070980, 2024.

882 883

Faranda, D., Messori, G., and Yiou, P.: Dynamical proxies of North Atlantic predictability and extremes, Sci Rep, 7, 41278, https://doi.org/10.1038/srep41278, 2017.

886

Faranda, D., Bourdin, S., Ginesta, M., Krouma, M., Noyelle, R., Pons, F., Yiou, P., and Messori, G.: A climate-change attribution retrospective of some impactful weather extremes of 2021, Weather Clim. Dynam., 3, 1311–1340, https://doi.org/10.5194/wcd-3-1311-2022, 2022.

890

Faranda, D., Ginesta, M., Alberti, T., Coppola, E., and Anzidei, M.: Attributing Venice Acqua Alta events to a changing climate and evaluating the efficacy of MoSE adaptation strategy, npj Clim Atmos Sci, 6, 181, https://doi.org/10.1038/s41612-023-00513-0, 2023a.

894

Faranda, D., Messori, G., Coppola, E., Alberti, T., Vrac, M., Pons, F., Yiou, P., Saint Lu, M., Hisi, A. N. S., Brockmann, P., Dafis, S., Mengaldo, G., and Vautard, R.: ClimaMeter: contextualizing extreme weather in a changing climate, Weather Clim. Dynam., 5, 959–983, https://doi.org/10.5194/wcd-5-959-2024, 2024.

899

900 Ferrarin, C., Pantillon, F., Davolio, S., Bajo, M., Miglietta, M. M., Avolio, E., Carrió, D. S., 901 Pytharoulis, I., Sanchez, C., Patlakas, P., González-Alemán, J. J., and Flaounas, E.: Assessing the coastal hazard of Medicane Ianos through ensemble modelling, Nat. Hazards Earth Syst. Sci., 23, 2273–2287, https://doi.org/10.5194/nhess-23-2273-2023, 2023a.

904

Ferrarin, C., Orlić, M., Bajo, M., Davolio, S., Umgiesser, G., and Lionello, P.: The contribution of a
mesoscale cyclone and associated meteotsunami to the exceptional flood in Venice on November 12,
Quart J Royal Meteoro Soc, 149, 2929–2942, https://doi.org/10.1002/qj.4539, 2023b.

908

Flaounas, E., Raveh-Rubin, S., Wernli, H., Drobinski, P., and Bastin, S.: The dynamical structure of intense Mediterranean cyclones, Clim Dyn, 44, 2411–2427, https://doi.org/10.1007/s00382-014-2330-2, 2015.

912

913 Flaounas, E., Di Luca, A., Drobinski, P., Mailler, S., Arsouze, T., Bastin, S., Beranger, K., and 914 Lebeaupin Brossier, C.: Cyclone contribution to the Mediterranean Sea water budget, Clim Dyn, 46, 915 913–927, https://doi.org/10.1007/s00382-015-2622-1, 2016.

916

917 Flaounas, E., Kotroni, V., Lagouvardos, K., Gray, S. L., Rysman, J.-F., and Claud, C.: Heavy rainfall 918 in Mediterranean cyclones. Part I: contribution of deep convection and warm conveyor belt, Clim 919 Dyn, 50, 2935–2949, https://doi.org/10.1007/s00382-017-3783-x, 2018.

920

Flaounas, E., Fita, L., Lagouvardos, K., and Kotroni, V.: Heavy rainfall in Mediterranean cyclones, Part II: Water budget, precipitation efficiency and remote water sources, Clim Dyn, 53, 2539–2555, https://doi.org/10.1007/s00382-019-04639-x, 2019.

924

Flaounas, E., Gray, S. L., and Teubler, F.: A process-based anatomy of Mediterranean cyclones: from baroclinic lows to tropical-like systems, Weather Clim. Dynam., 2, 255–279, https://doi.org/10.5194/wcd-2-255-2021, 2021.

927 https://doi.org/10.5194/wcu-2-255-2021, 2021

- 929 Flaounas, E., Davolio, S., Raveh-Rubin, S., Pantillon, F., Miglietta, M. M., Gaertner, M. A., Hatzaki,
- 930 M., Homar, V., Khodayar, S., Korres, G., Kotroni, V., Kushta, J., Reale, M., and Ricard, D.:
- 931 Mediterranean cyclones: current knowledge and open questions on dynamics, prediction, climatology 932 and impacts, Weather Clim. Dynam., 3, 173–208, https://doi.org/10.5194/wcd-3-173-2022, 2022.

933

- 934 Flaounas, E., Aragão, L., Bernini, L., Dafis, S., Doiteau, B., Flocas, H., Gray, S. L., Karwat, A.,
- 935 Kouroutzoglou, J., Lionello, P., Miglietta, M. M., Pantillon, F., Pasquero, C., Patlakas, P., Picornell,
- 936 M. Á., Porcù, F., Priestley, M. D. K., Reale, M., Roberts, M. J., Saaroni, H., Sandler, D., Scoccimarro,
- 937 E., Sprenger, M., and Ziv, B.: A composite approach to produce reference datasets for extratropical
- 938 cyclone tracks: application to Mediterranean cyclones, Weather Clim. Dynam., 4, 639–661,
- https://doi.org/10.5194/wcd-4-639-2023, 2023. 939

940

- 941 Grimaldi, S., Salamon, P., Disperati, J., Zsoter, E., Russo, C., Ramos, A., Carton De Wiart, C.,
- 942 Barnard, C., Hansford, E., Gomes, G., Prudhomme, C. (2022): River discharge and related historical
- 943 data from the Global Flood Awareness System. v4.0. European Commission, Joint Research Centre
- 944 (JRC). URL: https://cds.climate.copernicus.eu/cdsapp#!/dataset/cems-glofas-historical (Accessed on
- 945 09-Oct-2023)

946

- 947 Global Data Institute of the UN International Organization for Migration (IOM). 2023. Libya —
- 948 Storm Daniel Flash update 3 (14 September 2023)

949

- 950 He, K., Yang, Q., Shen, X., Dimitriou, E., Mentzafou, A., Papadaki, C., Stoumboudi, M., and
- 951 Anagnostou, E. N.: Brief communication: Storm Daniel Flood Impact in Greece 2023: Mapping Crop
- 952 and Livestock Exposure from SAR, https://doi.org/10.5194/nhess-2023-173, 12 October 2023.

953

- 954 Hersbach, H., Bell, B., Berrisford, P., Hirahara, S., Horányi, A., Muñoz-Sabater, J., Nicolas, J.,
- 955 Peubey, C., Radu, R., Schepers, D., Simmons, A., Soci, C., Abdalla, S., Abellan, X., Balsamo, G.,
- 956 Bechtold, P., Biavati, G., Bidlot, J., Bonavita, M., De Chiara, G., Dahlgren, P., Dee, D., Diamantakis,
- 957 M., Dragani, R., Flemming, J., Forbes, R., Fuentes, M., Geer, A., Haimberger, L., Healy, S., Hogan,
- 958 R. J., Hólm, E., Janisková, M., Keeley, S., Laloyaux, P., Lopez, P., Lupu, C., Radnoti, G., De Rosnay,
- 959 P., Rozum, I., Vamborg, F., Villaume, S., and Thépaut, J.: The ERA5 global reanalysis, Quart J Royal 960 Meteoro Soc, 146, 1999–2049, https://doi.org/10.1002/qj.3803, 2020.

961

- 962 Hewson, T., Ashoor, A., Boussetta, S., Emanuel, K., Lagouvardos, K., Lavers, D., Magnusson, L.,
- 963 Pillosu, F., Zsoter, E., Medicane Daniel: an extraordinary cyclone with devastating impacts, ECMWF
- 964 newsletters 179, 2024, 33-47.

965

- 966 Hochman, A., Scher, S., Quinting, J., Pinto, J. G., and Messori, G.: Dynamics and predictability of 967 over the Eastern Mediterranean, Clim Dyn, 58, 2047–2064,
- 968 https://doi.org/10.1007/s00382-020-05465-2, 2022a. 969

- 970 Hochman, A., Marra, F., Messori, G., Pinto, J. G., Raveh-Rubin, S., Yosef, Y., and Zittis, G.: Extreme
- 971 weather and societal impacts in the eastern Mediterranean, Earth Syst. Dynam., 13, 749-777,
- 972 https://doi.org/10.5194/esd-13-749-2022, 2022b.

973

- 974 Hochman, A., Plotnik, T., Marra, F., Shehter, E.-R., Raveh-Rubin, S., and Magaritz-Ronen, L.: The
- 975 sources of extreme precipitation predictability; the case of the 'Wet' Red Sea Trough, Weather and
- 976 Climate Extremes, 40, 100564, https://doi.org/10.1016/j.wace.2023.100564, 2023.

977

- 978 Hochman, A., Shachar, N., and Gildor, H.: Unraveling sub-seasonal precipitation variability in the
- 979 East via Indian Ocean sea surface temperature, Sci Rep, 2919,
- 980 https://doi.org/10.1038/s41598-024-53677-x, 2024.

982 IFRC (International Federation of Red Cross and Red Crescent Societies). World Disasters Report 983 2020 Executive Summary. https://www.ifrc.org/document/world-disasters-report-2020

984

985 Khodayar, S., Davolio, S., Di Girolamo, P., Lebeaupin Brossier, C., Flaounas, E., Fourrie, N., Lee, 986 K.-O., Ricard, D., Vie, B., Bouttier, F., Caldas-Alvarez, A., and Ducrocq, V.: Overview towards 987 improved understanding of the mechanisms leading to heavy precipitation in the western 988 Mediterranean: lessons learned from HyMeX, Atmos. Chem. Phys., 21, 17051–17078, 989 https://doi.org/10.5194/acp-21-17051-2021, 2021.

990

991 Korres, G., Ravdas, M., Denaxa, D., & Sotiropoulou, M. (2021). Mediterranean Sea Waves 992 Reanalysis INTERIM (CMEMS Med-Waves, MedWAM3I system) (Version 1) [Data set]. 993 Copernicus Monitoring Environment Marine Service (CMEMS). 994 https://doi.org/10.25423/CMCC/MEDSEA_MULTIYEAR_WAV_006_012_MEDWAM3I

995

996 Korres, G., Oikonomou, C., Denaxa, D., & Sotiropoulou, M. (2023). Mediterranean Sea Waves 997 Analysis and Forecast (Copernicus Marine Service MED-Waves, MEDWAM4 system) (Version 1) 998 [Data set]. Copernicus Marine Service (CMS). 999 https://doi.org/10.25423/CMCC/MEDSEA_ANALYSISFORECAST_WAV_006_017_MEDWAM4

1000

1001 Lagouvardos, K., Kotroni, V., Bezes, A., Koletsis, I., Kopania, T., Lykoudis, S., Mazarakis, N., 1002 Papagiannaki, K., and Vougioukas, S.: The automatic weather stations NOANN network of the 1003 National Observatory of Athens: operation and database, Geoscience Data Journal, 4, 4–16, 1004 https://doi.org/10.1002/gdj3.44, 2017.

1005

1006 Messmer, M., Gómez-Navarro, J. J., and Raible, C. C.: Sensitivity experiments on the response of Vb 1007 cyclones to sea surface temperature and soil moisture changes, Earth Syst. Dynam., 8, 477-493, 1008 https://doi.org/10.5194/esd-8-477-2017, 2017.

1009

1010 Miglietta, M. M., Moscatello, A., Conte, D., Mannarini, G., Lacorata, G., and Rotunno, R.: Numerical 1011 analysis of a Mediterranean 'hurricane' over south-eastern Italy: Sensitivity experiments to sea 1012 temperature, Atmospheric Research, surface 101, 412–426, 1013 https://doi.org/10.1016/j.atmosres.2011.04.006, 2011.

1014

1015 Miglietta, M. M., Carnevale, D., Levizzani, V., and Rotunno, R.: Role of moist and dry air advection 1016 in the development of Mediterranean tropical-like cyclones (medicanes), Quart J Royal Meteoro Soc, 1017 147, 876–899, https://doi.org/10.1002/qj.3951, 2021. 1018

1019 Miglietta M. M., González-Alemán J. J., Panegrossi G., Gaertner M. A., Pantillon F., Pasquero C., 1020 Schultz D. M., D'Adderio L. P., Dafis S., Husson R., Ricchi A., Carrió D. S., Davolio S., Fita L., 1021 Picornell M. A., Pytharoulis I., Raveh-Rubin S., Scoccimarro E., Bernini L., Cavicchia L., Conte D., 1022 Ferretti R., Flocas H., Gutiérrez-Fernández J., Hatzaki M., Homar Santaner V., Jansà A., Patlakas P., 1023 Flaounas E., Defining Medicanes: Bridging the Knowledge Gap Between Tropical and Extratropical 1024 Cyclones in the Mediterranean, Bull. Am. Meteor. Soc., submitted

1025

1026 Nissen, K. M., Leckebusch, G. C., Pinto, J. G., Renggli, D., Ulbrich, S., and Ulbrich, U.: Cyclones 1027 causing wind storms in the Mediterranean: characteristics, trends and links to large-scale patterns, 1028 Nat. Hazards Earth Syst. Sci., 10, 1379–1391, https://doi.org/10.5194/nhess-10-1379-2010, 2010.

1029

1030 Pantillon, F. P., Chaboureau, J.-P., Mascart, P. J., and Lac, C.: Predictability of a Mediterranean 1031 Tropical-Like Storm Downstream of the Extratropical Transition of Hurricane Helene (2006), 1032 Monthly Weather Review, 141, 1943–1962, https://doi.org/10.1175/MWR-D-12-00164.1, 2013.

1033

1034 Pantillon, F., Davolio, S., Avolio, E., Calvo-Sancho, C., Carrió, D. S., Dafis, S., Gentile, E. S., 1035 Gonzalez-Aleman, J. J., Gray, S., Miglietta, M. M., Patlakas, P., Pytharoulis, I., Ricard, D., Ricchi,

- A., Sanchez, C., and Flaounas, E.: The crucial representation of deep convection for the cyclogenesis
- 1037 of Medicane Ianos, Weather Clim. Dynam., 5, 1187–1205, https://doi.org/10.5194/wcd-5-1187-2024, 1038 2024.

1039

Patlakas, P., Stathopoulos, C., Tsalis, C., and Kallos, G.: Wind and wave extremes associated with tropical-like cyclones in the Mediterranean basin, Intl Journal of Climatology, 41, https://doi.org/10.1002/joc.6795, 2021.

1043

1044 Pfahl, S. and Wernli, H.: Quantifying the Relevance of Cyclones for Precipitation Extremes, Journal of Climate, 25, 6770–6780, https://doi.org/10.1175/JCLI-D-11-00705.1, 2012.

1046

Portal, A., Raveh-Rubin, S., Catto, J. L., Givon, Y., and Martius, O.: Linking compound weather extremes to Mediterranean cyclones, fronts, and airstreams, Weather Clim. Dynam., 5, 1043–1060, https://doi.org/10.5194/wcd-5-1043-2024, 2024.

1050

Pytharoulis, I.: Analysis of a Mediterranean tropical-like cyclone and its sensitivity to the sea surface temperatures, Atmospheric Research, 208, 167–179, https://doi.org/10.1016/j.atmosres.2017.08.009, 1053 2018.

1054

1055 Qiu J., Zhao W., Brocca L., Paolo Tarolli (2023). Storm Daniel revealed the fragility of the 1056 Mediterranean region. The Innovation Geoscience 1(3), 100036. https://doi.org/10.59717/j.xinn-1057 geo.2023.100036

1058

Raveh-Rubin, S. and Flaounas, E.: A dynamical link between deep Atlantic extratropical cyclones and intense Mediterranean cyclones, Atmospheric Science Letters, 18, 215–221, https://doi.org/10.1002/asl.745, 2017.

1062

Raveh-Rubin, S. and Wernli, H.: Large-scale wind and precipitation extremes in the Mediterranean: dynamical aspects of five selected cyclone events, Quart J Royal Meteoro Soc, 142, 3097–3114, https://doi.org/10.1002/qj.2891, 2016.

1066

Reale, M., Cabos Narvaez, W. D., Cavicchia, L., Conte, D., Coppola, E., Flaounas, E., Giorgi, F., Gualdi, S., Hochman, A., Li, L., Lionello, P., Podrascanin, Z., Salon, S., Sanchez-Gomez, E., Scoccimarro, E., Sein, D. V., and Somot, S.: Future projections of Mediterranean cyclone characteristics using the Med-CORDEX ensemble of coupled regional climate system models, Clim Dyn, 58, 2501–2524, https://doi.org/10.1007/s00382-021-06018-x, 2022.

1072

Ricchi, A.,Miglietta, M. M., Barbariol, F., Benetazzo, A., Bergamasco, A., Bonaldo, D., Cassardo, C., Falcieri, F. M., Modugno, G., Russo, A., Sclavo, M., and Carniel, S.: Sensitivity of a Mediterranean tropical-like cyclone to different model configurations and coupling strategies, Atmosphere, 8, 1–32, https://doi.org/10.3390/atmos8050092, 2017.

1077

1078 Romero, R. and Emanuel, K.: Climate Change and Hurricane-Like Extratropical Cyclones: 1079 Projections for North Atlantic Polar Lows and Medicanes Based on CMIP5 Models, J. Climate, 30, 279–299, https://doi.org/10.1175/JCLI-D-16-0255.1, 2017.

1081

Rousseau-Rizzi, R., Raveh-Rubin, S., Catto, J. L., Portal, A., Givon, Y., and Martius, O.: A storm-relative climatology of compound hazards in Mediterranean cyclones, Weather Clim. Dynam., 5, 1079–1101, https://doi.org/10.5194/wcd-5-1079-2024, 2024.

1085

Sanchez, C., Gray, S., Volonte', A., Pantillon, F., Berthou, S., and Davolio, S.: The impact of preceding convection on the development of Medicane Ianos and the sensitivity to sea surface temperature. Weather Clim. Dynam., 5, 1429 - 1455, https://doi.org/10.5194/wcd-5-1429-2024, 2024.

1089

1090 Scherrmann, A., Wernli, H., and Flaounas, E.: The upstream-downstream connection of North

Atlantic and Mediterranean cyclones in semi-idealized simulations, Weather Clim. Dynam., 5, 419–438, https://doi.org/10.5194/wcd-5-419-2024, 2024.

1093

Shirzaei, M., Vahedifard, F., Sadhasivam, N., Ohenhen, L., Dasho, O., Tiwari, A., Werth, S., Azhar, M., Zhao, Y., Nicholls, R. J., and AghaKouchak, A.: Aging dams, political instability, poor human

 $1096 \quad \text{decisions} \quad \text{and} \quad \text{climate} \quad \text{change:} \quad \text{recipe} \quad \text{for} \quad \text{human} \quad \text{disaster,} \quad \text{npj} \quad \text{Nat.} \quad \text{Hazards,} \quad 2, \quad 1-8, \quad \text{hazards,} \quad 1-8, \quad 1-8, \quad \text{hazards,} \quad 1-8,$

1097 https://doi.org/10.1038/s44304-024-00056-1, 2025.

1098

Sioni, F., Davolio, S., Grazzini, F., and Giovannini, L.: Revisiting the atmospheric dynamics of the two century floods over north-eastern Italy. Atmos. Research, 286, 106662, 1101 https://doi.org/10.1016/j.atmosres.2023.106662, 2023.

1102

Sodemann, H., Schwierz, C., and Wernli, H.: Interannual variability of Greenland winter precipitation sources: Lagrangian moisture diagnostic and North Atlantic Oscillation influence, J. Geophys. Res., 1105 113, 2007JD008503, https://doi.org/10.1029/2007JD008503, 2008.

1106

1107 Sprenger, M. and Wernli, H.: The LAGRANTO Lagrangian analysis tool – version 2.0, Geosci. 1108 Model Dev., 8, 2569–2586, https://doi.org/10.5194/gmd-8-2569-2015, 2015.

1109

1110 UNICEF. 2023. Libya Storm Daniel & Flooding, Situation Report #1. (14-09-2023)

1111

1112 United Nations Office for the Coordination of Humanitarian Affairs (OCHA). 2023. Flash Appeal1113 Libya.

1114

Varlas, G., Vervatis, V., Spyrou, C., Papadopoulou, E., Papadopoulos, A., and Katsafados, P.: Investigating the impact of atmosphere—wave—ocean interactions on a Mediterranean tropical-like cyclone, Ocean Model., 153, 101675, https://doi.org/10.1016/j.ocemod.2020.101675, 2020.

1118

1119 Vito Romaniello, Paolo Oddo, Marina Tonani, Lucio Torrisi, Alessandro Grandi, and Nadia Pinardi: 1120 Impact of Sea Surface Temperature on COSMO Forecasts of a Medicane over the Western

1121 Mediterranean Sea, JEASE, 5, https://doi.org/10.17265/2159-581X/2015.06.002, 2015.

1122

Weather Meteorological Organisation: https://wmo.int/media/news/libya-floods-show-need-multi-hazard-early-warnings-unified-response, last access: 10 March 2024.

1125

Weather Meteorological Organisation: https://wmo.int/media/news/storm-daniel-leads-extreme-rain-and-floods-mediterranean-heavy-loss-of-life-libya, last access: 3 February, 2025

1128

Wernli, H. and Davies, H. C.: A Lagrangian-based analysis of extratropical cyclones. I: The method and some applications, Quart J Royal Meteoro Soc, 123, 467–489, https://doi.org/10.1002/qj.49712353811, 1997.

1132

World Bank, 2023. Libya Storm and Flooding 2023. Rapid Damage and Needs Assessment. Washington, DC: World Bank, http://recovery.preventionweb.net/quick/82808.

1135

- 1138
- 1139
- 1140
- 1141
- 1142
- 1143
- 1144
- 1145

Figures

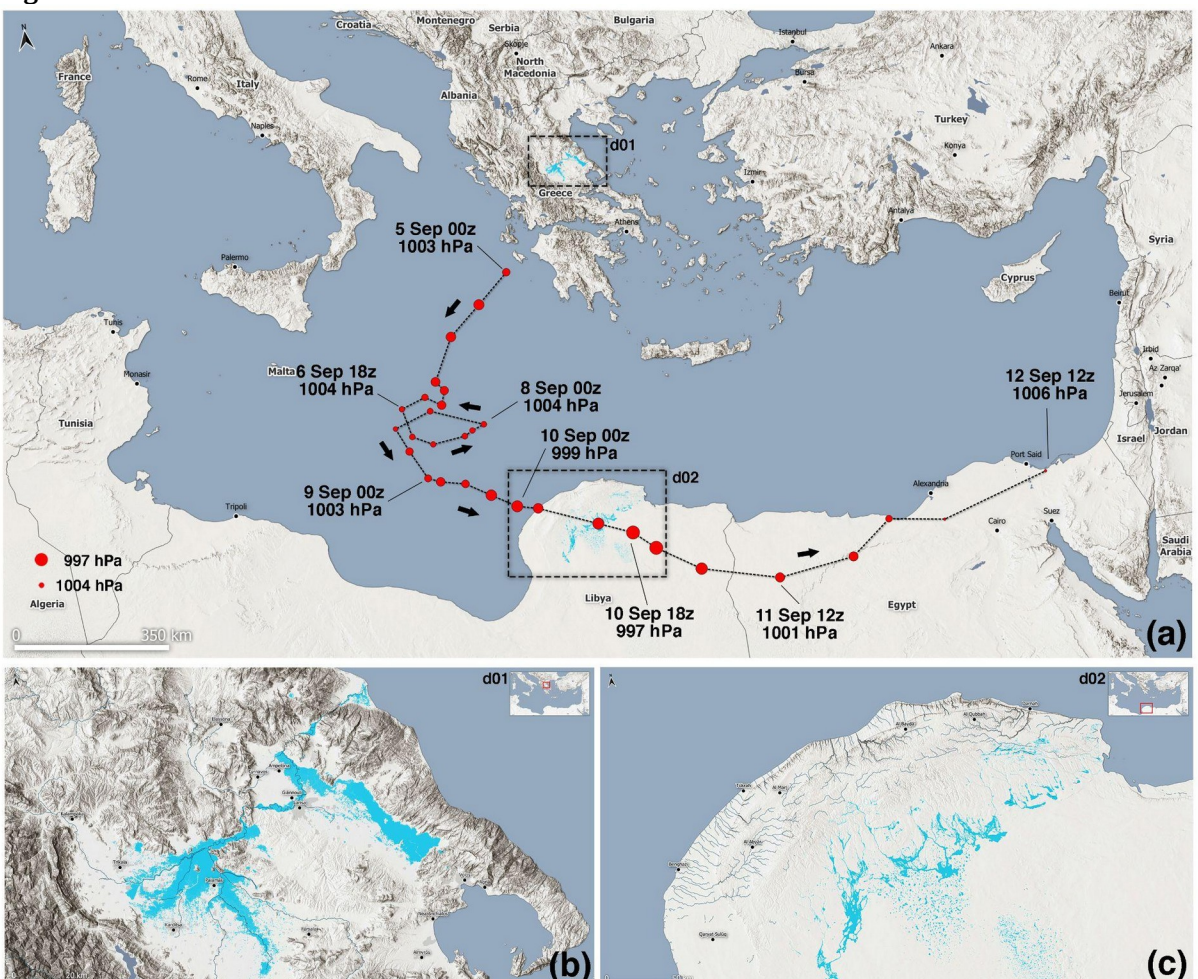


Figure 1 (a) Track of Storm Daniel at six-hour intervals based on ECMWF analysis, where the size of red dots is proportional to cyclone depth in terms of minimum mean sea level pressure. Flooded areas are shown in cyan and blue tones (acquired by one of the Copernicus Sentinel-2 satellites on 10 and 12 September 2023). Panels (b) and (c) zoom over central Greece and Libya (square boxes in panel **a**).

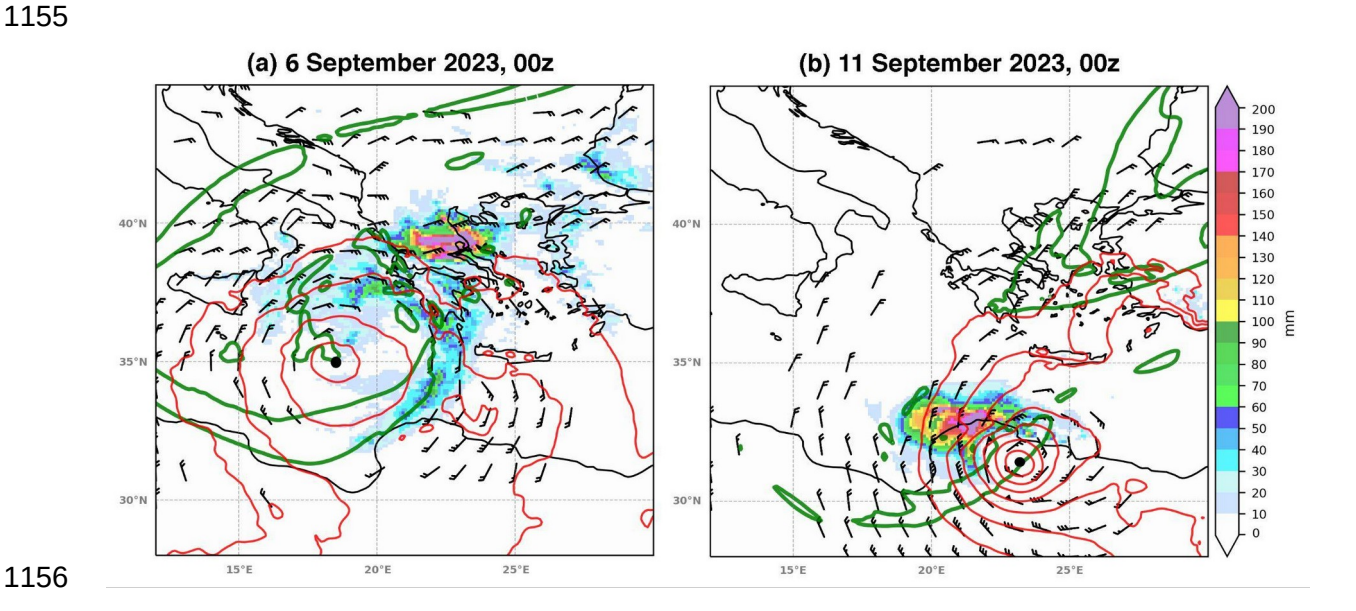


Figure 2 (a) Potential Vorticity of 2 PVU at 300 hPa (in green contour) and wind speed higher than 15 knots at 850 hPa (in barbs, with full and half bars depicting 10 and 5 knots, respectively) and mean sea level pressure (in red contours for values lower than 1012 hPa with 2 hPa interval) on 6 September 2023, at 00 UTC. 24-hour total accumulated precipitation from 5 to 6 of September 00 UTC is shown in shading (max value 434 mm). **(b)** Same as **(a)** but for 11 September 2023, at 00 UTC (max precipitation value 382 mm). The black dot indicates the minimum sea level pressure position in both panels.

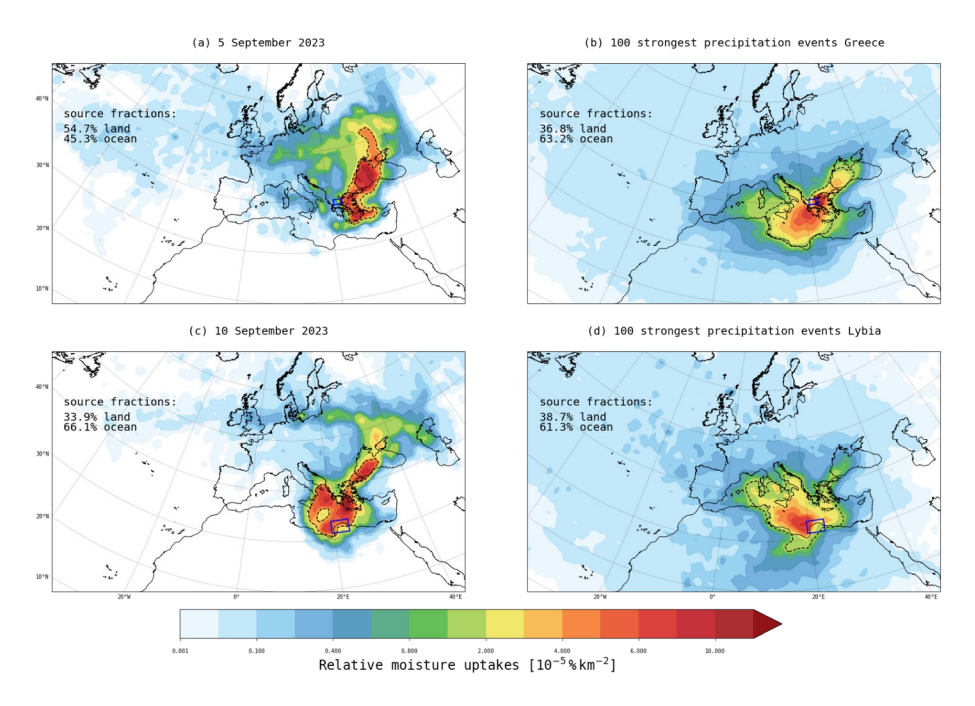


Figure 3 (a) Relative moisture uptakes that contribute to the precipitation event in Thessaly (depicted with the blue rectangle) on 5 September 2023. The black dashed contour outlines the largest moisture source regions, which account for 50% of the total moisture uptake. The numbers on the top left show the relative land and ocean fraction of the moisture sources. **(b)** as in **(a)** but for the 100 most extreme daily precipitation events in Thessaly from 1990 to 2023. **(c)** as in **(a)** but for the precipitation in the study region in Libya (blue rectangle) on 10 September 2023. **(d)** as in **(b)** but for Libya.

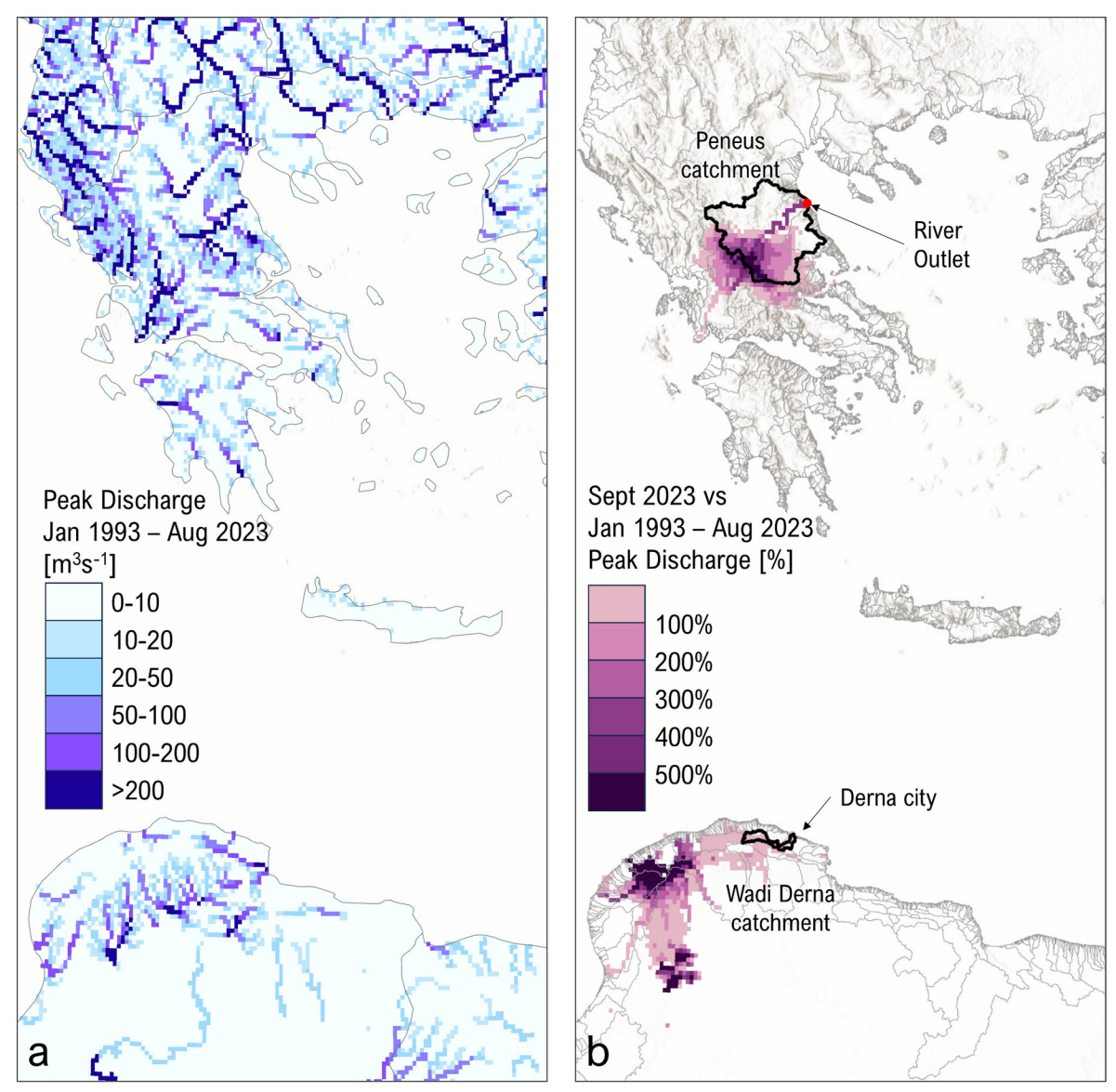


Figure 4 Peak discharge over three recent decades (Jan 1993 – Aug 2023) versus Daniel storm as represented by the Global Flood Awareness System (**a**) spatial distribution of the maximum peak river discharge from January 1993 to August 2023, (**b**) comparison map for September 2023 illustrating the event-wide peak discharges as a percentage increase over the maximum peak discharges during the 30 years January in (**a**).

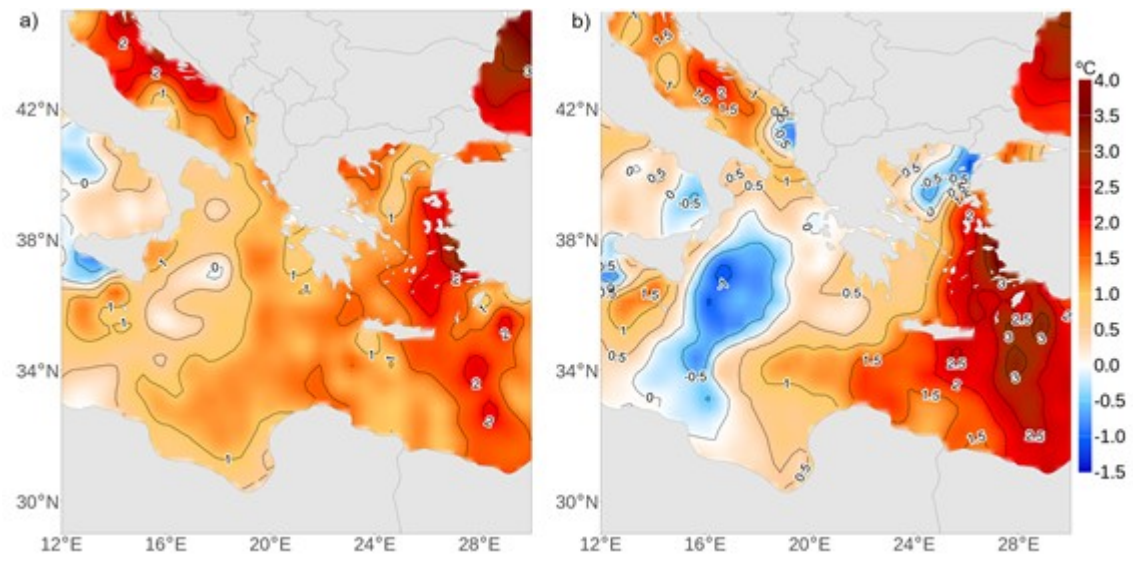


Figure 5 (a) Daily SST anomaly from ERA5, for 3 September 2023, and (b) 9 September 2023. The reference climatology for anomaly determination is 1982-2011.

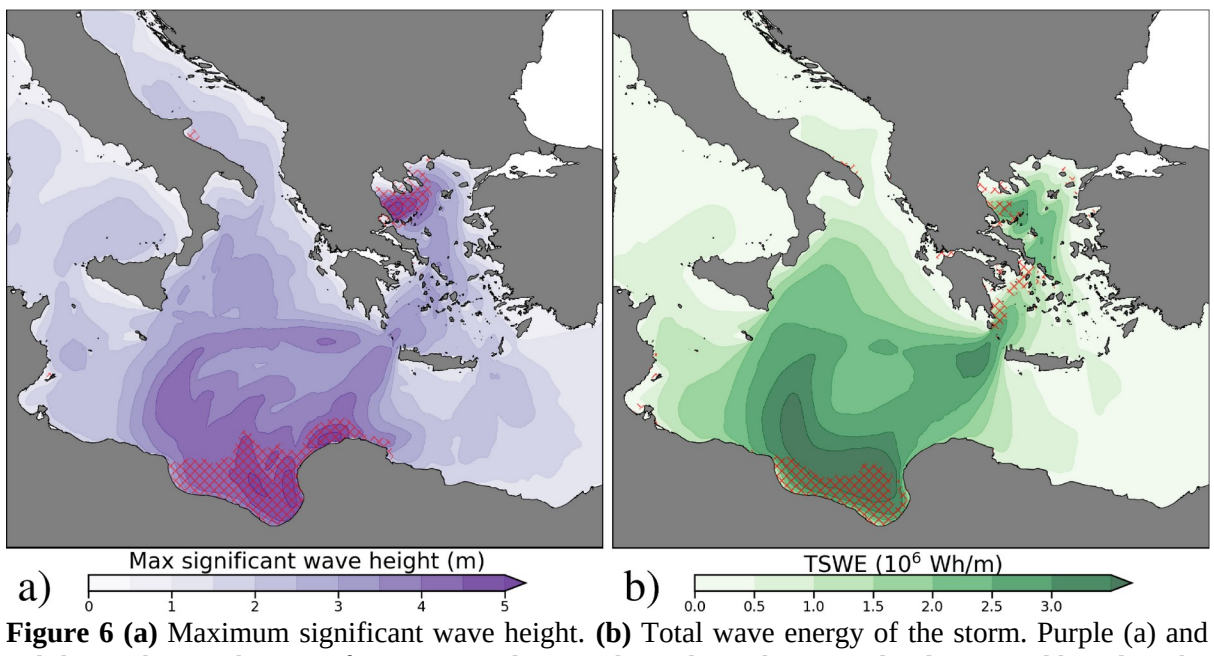


Figure 6 (a) Maximum significant wave height. **(b)** Total wave energy of the storm. Purple (a) and red (b) patches mark areas of extreme conditions (above the 99th percentile) determined based on the Mediterranean Sea wave reanalysis.

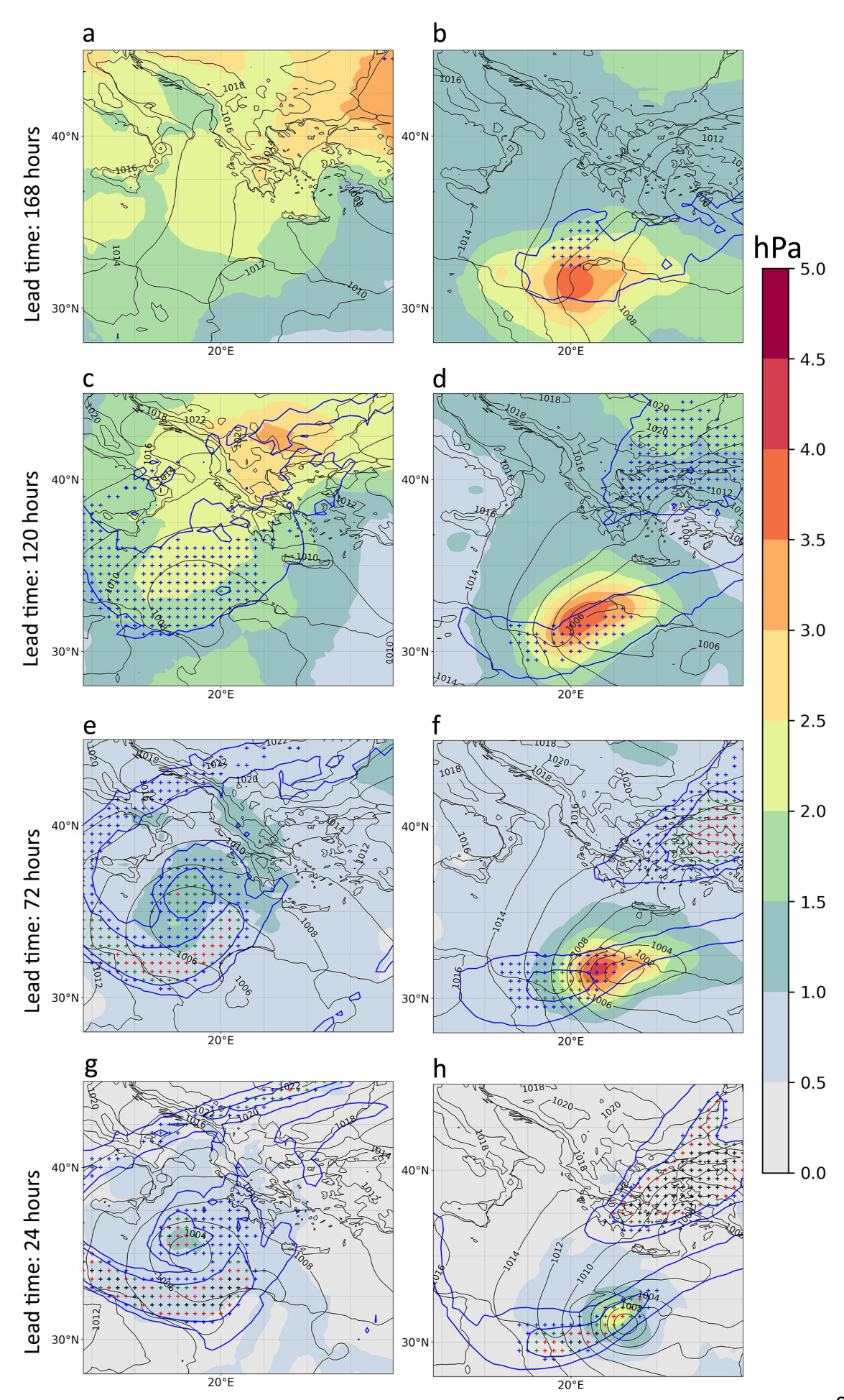


Figure 7 Standard deviation (in colour) and average (in black contour) MSLP from the 51 ensemble members of the ECMWF EPS. Blue contours enclose areas with a median equal to 1 and 2 PVU at 300 hPa among all members of the EPS. Blue crosses indicate areas where at least 25% of the members have PV values greater than 2 PVU. Green, red, and black crosses denote agreement by at least 50%, 75%, and 95% of the members, respectively. Panels depict different lead forecast times valid on 6 September at 00 UTC (panels **a**, **c**, **e**, **g**) and 11 September at 00 UTC (**b**, **d**, **f**, **h**).

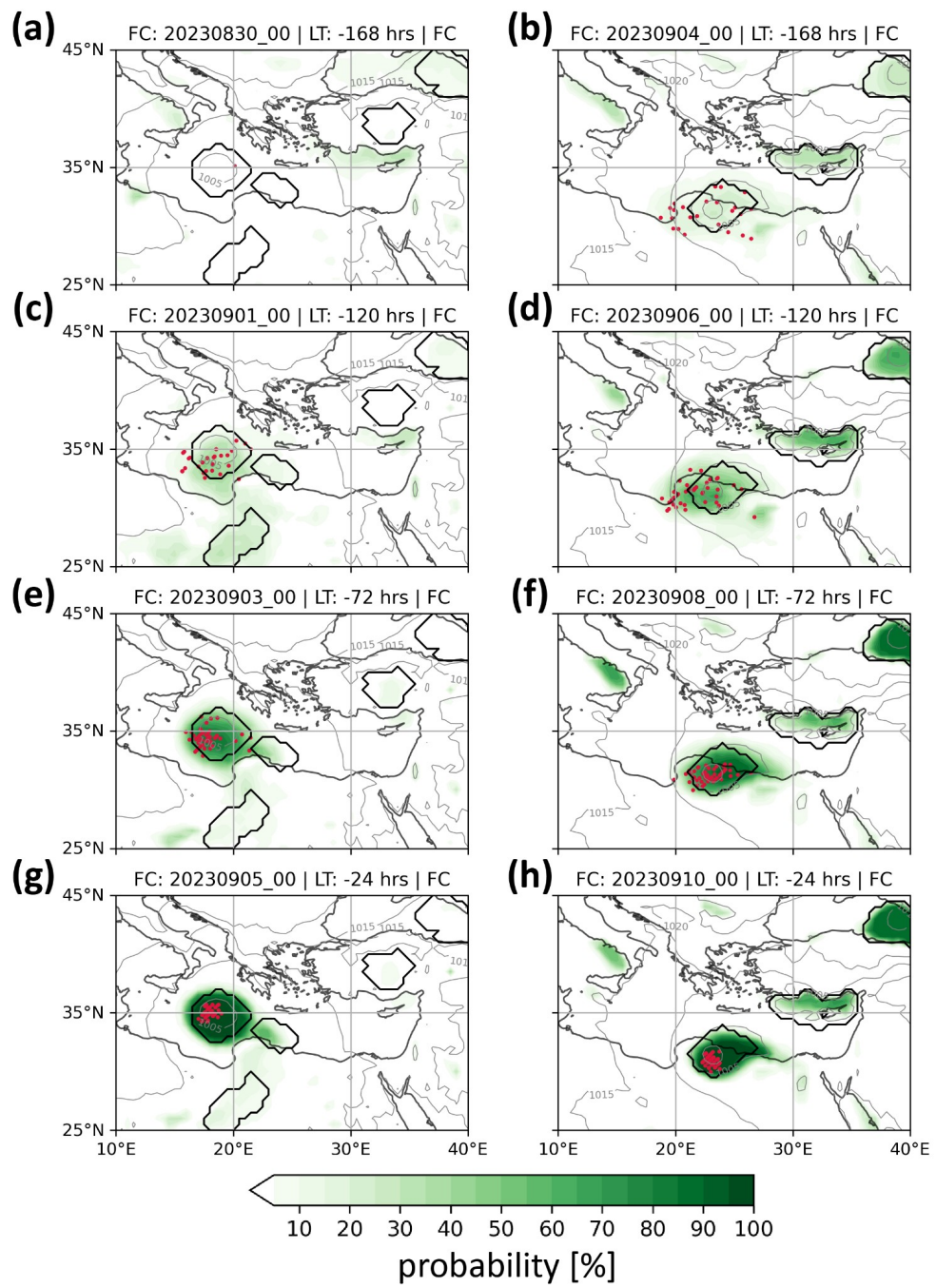


Figure 8 Percentage of overlapping cyclone objects (green shading) among the ensemble prediction system members for different lead times valid on 6 September 2023, 00 UTC (left column panels) and 11 September 2023, 00 UTC (right column panels). Black contours show cyclone objects in ECMWF analysis (grey contours for MSLP isobars in ECMWF analysis). Red dots depict the location of the minimum pressure of Daniel in the ensemble members.

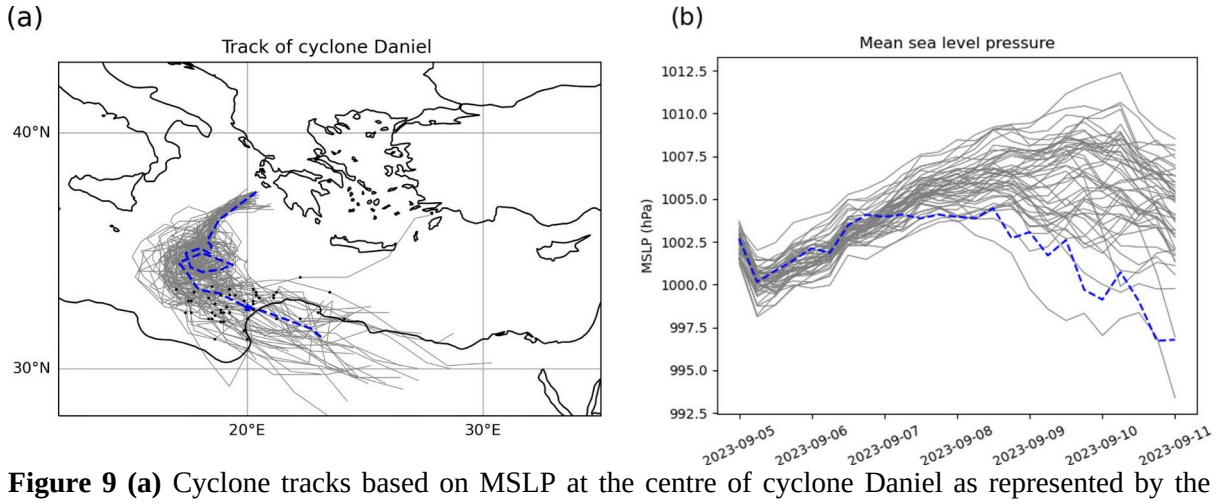


Figure 9 (a) Cyclone tracks based on MSLP at the centre of cyclone Daniel as represented by the ECMWF analysis (blue dashed line) and by the 50 members of the EPS of ECMWF (grey lines), initialized on 5 September at 00 UTC. Black dots in (a) depict the cyclone location on 10 September, 00 UTC (b) As in (a) but as time series of minimum MSLP.

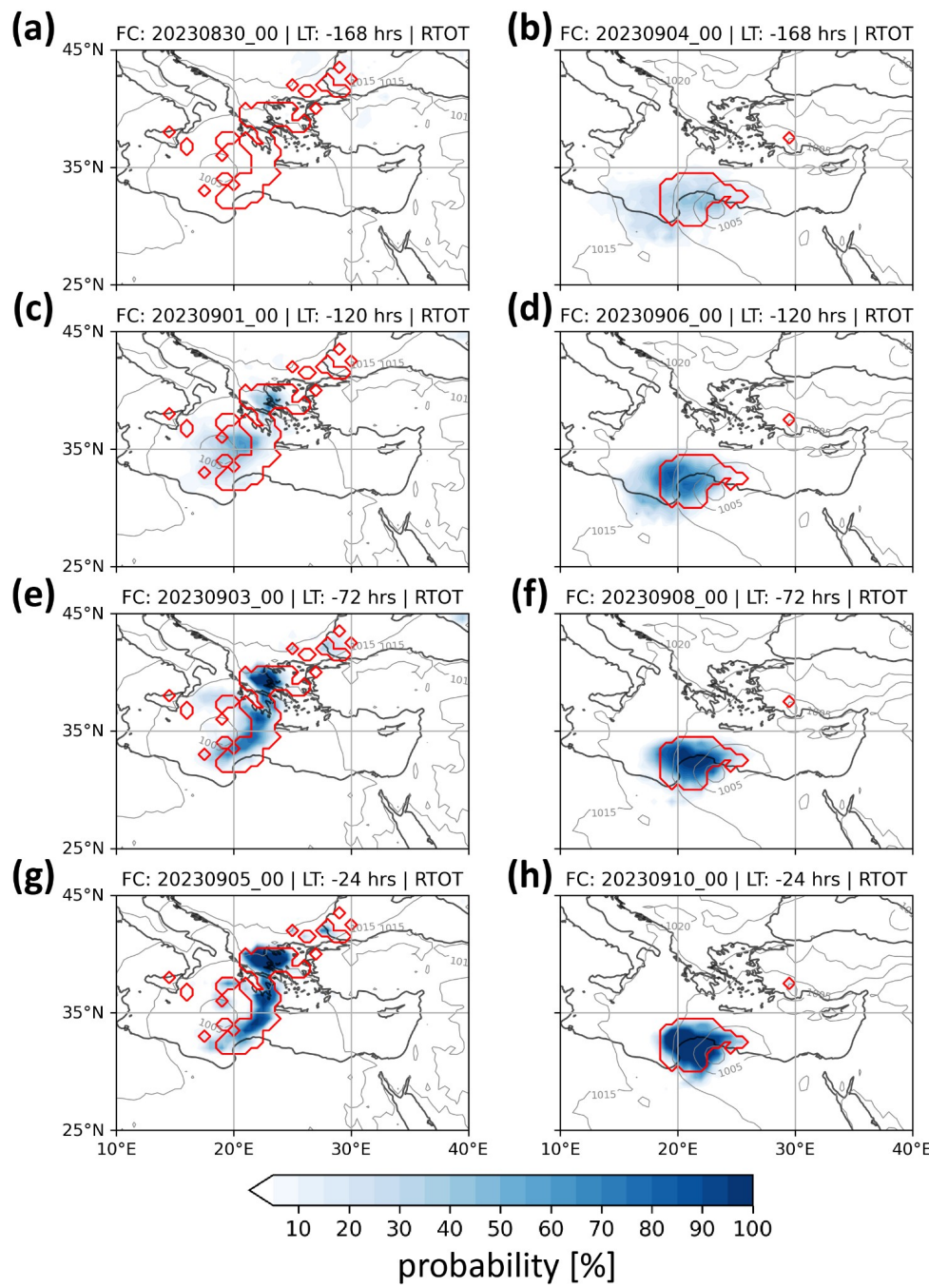


Figure 10 Percentage of overlapping objects (in blue shading) among the ensemble prediction members for 24-hour accumulation (ending at the validity time) of extreme precipitation for different lead times valid on 6 September 2023, 00 UTC (left column panels) and 11 September 2023, 00 UTC (right column panels). Red contours show objects of extreme precipitation determined based on ERA5 climatology (grey contours for MSLP isobars in ECMWF analysis).

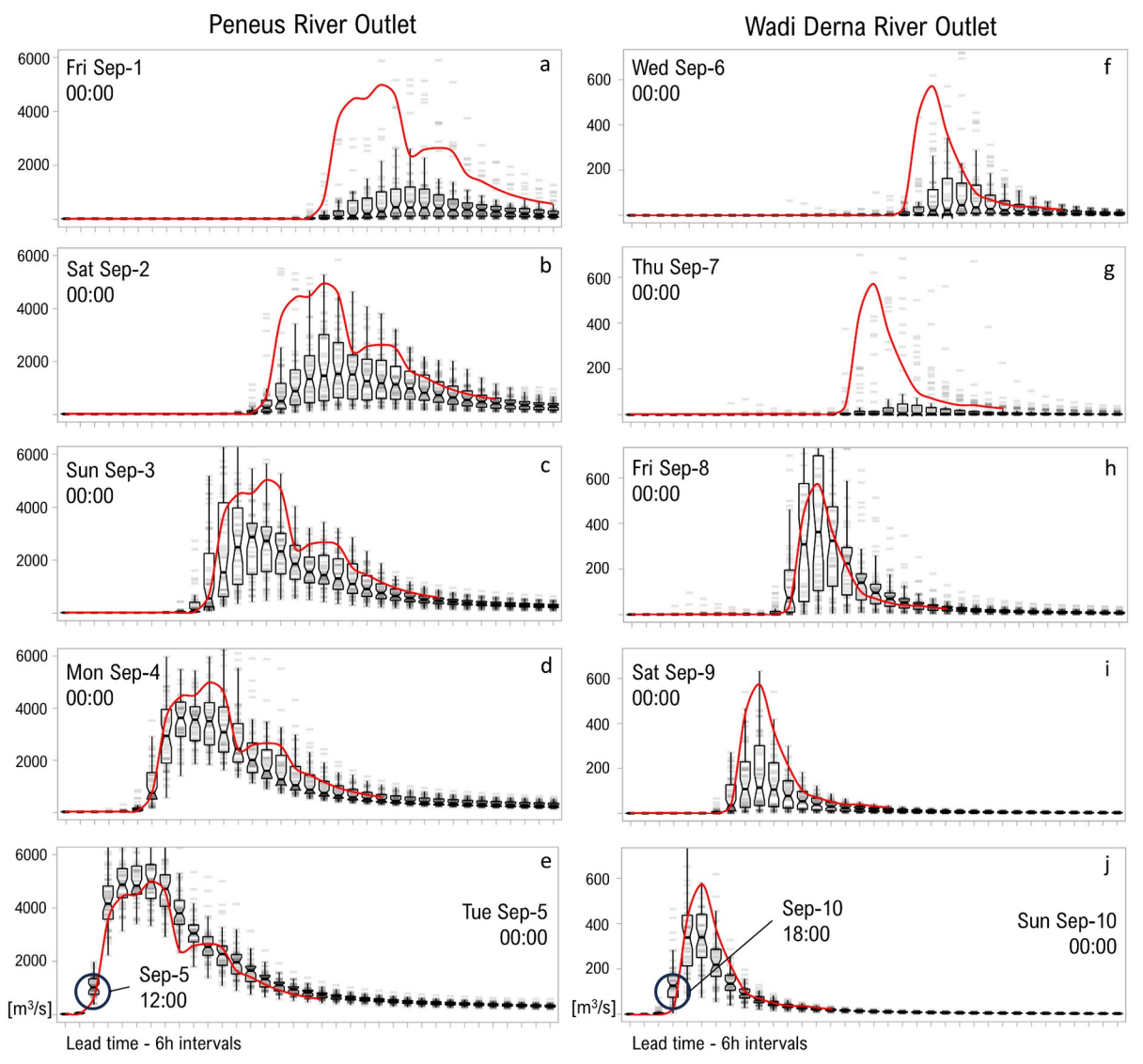


Figure 11 Six-hourly ensemble river discharge forecasts for the Peneus and Wadi Derna catchments compared to the "perfect forecast" benchmark (red line). The "perfect forecast" represents the initialization of each forecast for all time steps across the event, taken as a reference for evaluating forecast accuracy. With the observed timing of rising hydrograph limbs marked on 5 September, noon local time (09 UTC) for the Peneus River in Thessaly, and 10 September, 18:00 local time (16 UTC) for the Wadi Derna River. Grey stripes (tick marks) represent individual ensemble members from the EFAS model, driven by the 51 ensemble members of the ECMWF EPS. Overlapping tick marks darken, visually highlighting areas of member agreement (convergence). Forecast summary data are displayed as boxplots, where the box represents the interquartile range (IQR), the whiskers show the range of values within 1.5 times the IQR, and the horizontal black line inside the box indicates the median. The notches around the median show the 95% confidence interval.

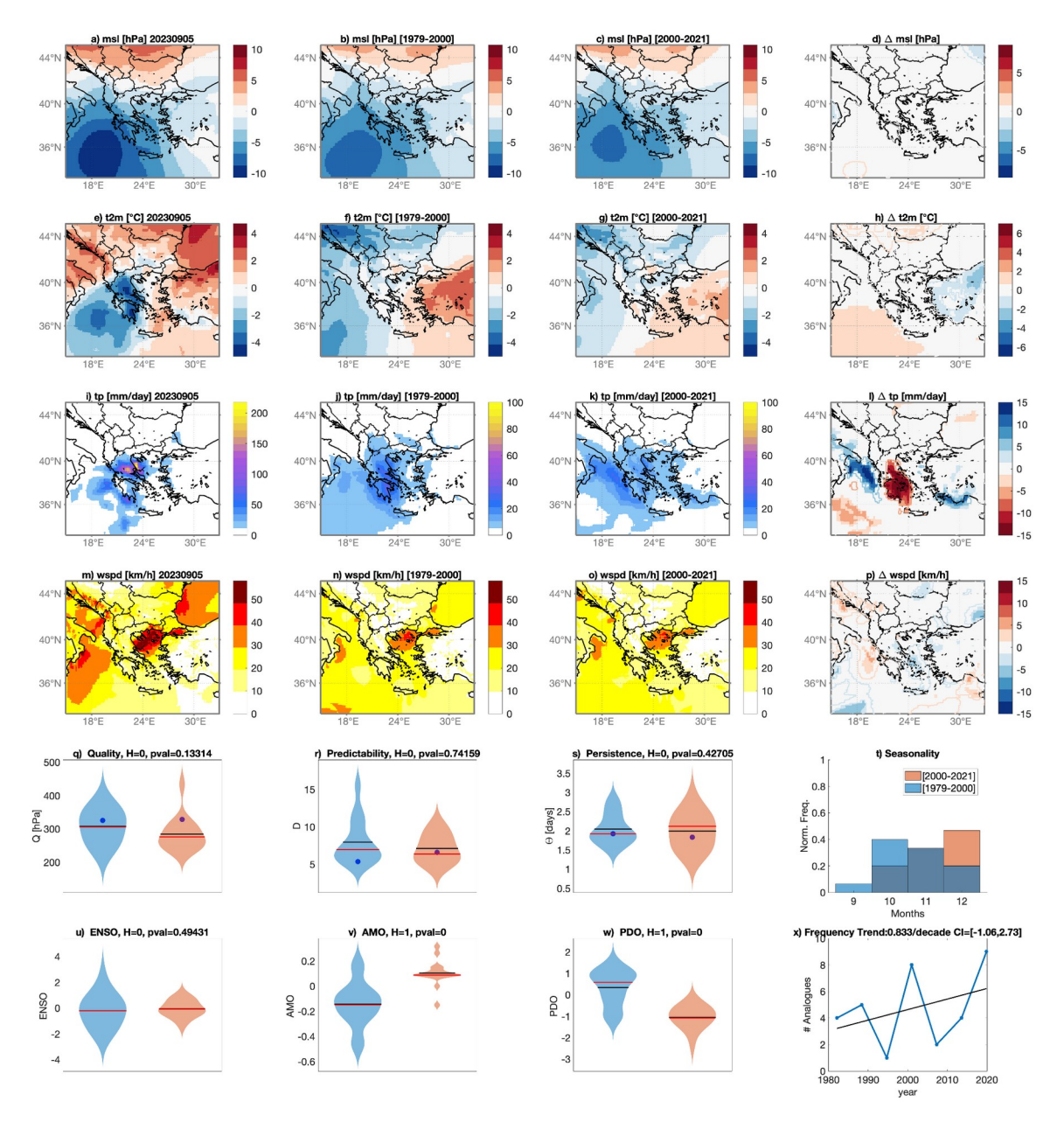


Figure 12: Analogues for 5 September 2023 and the region [15°E-33°E, 33°N-45°N] and the extended summer season SOND: average surface pressure anomaly (msl) (a), average 2-m temperature anomalies (t2m) (e), accumulated total precipitation (tp) (i), and average wind-speed (wspd) in the period of the event. Average of the surface pressure analogs found in the counterfactual [1979-2000] (b) and factual periods [2001-2022] (c), along with corresponding 2-m temperatures (f, g), accumulated precipitation (j, k), and wind speed (n, o). Changes between present and past analogs are presented for surface pressure Δslp (d), 2-m temperatures Δ t2m (h), total precipitation Δ tp (i), and windspeed Δ wspd (p): color-filled shaded areas indicate significant anomalies obtained from the bootstrap procedure. Contours indicate non-significant changes; Violin plots for past (blue) and present (orange) periods for Quality Q analogs (q), Predictability Index D (r), Persistence Index Θ (s), and distribution of analogs in each month (t). Violin plots for past (blue) and present (orange) periods for ENSO (u), AMO (v) and PDO (w). Number of the Analogues occurring in each subperiod (blue) and linear trend (black). A blue dot marks values for the peak day of the extreme event. Horizontal bars in panels (q,r,s,u,v,w) correspond to the mean (black) and median (red) of the distributions.

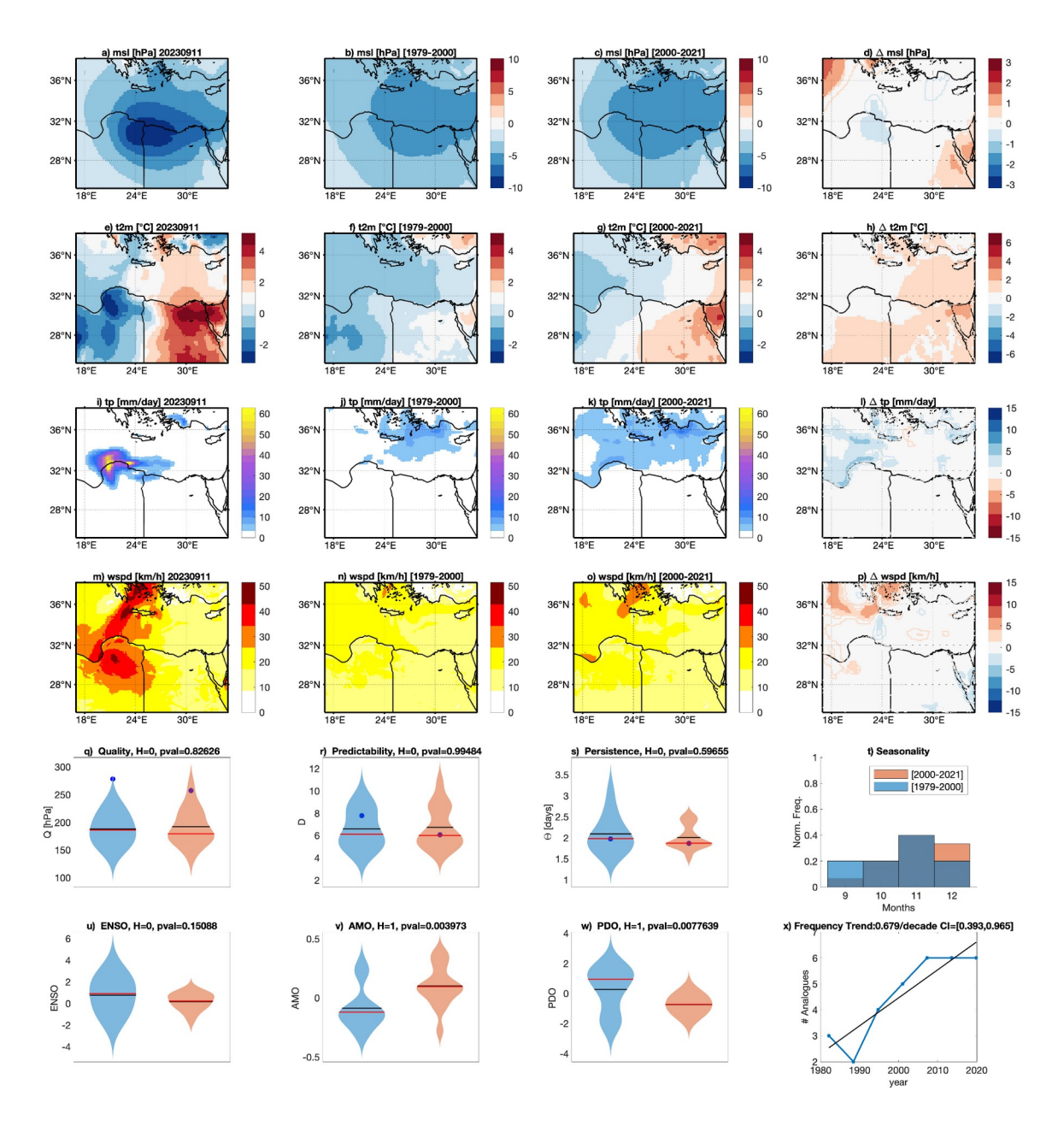


Figure 13: As in Fig. 12, but for 10-11 September 2023, the region [17°E-35°E, 25°N-38°N] and the extended autumn season (SOND).